Monte Carlo Methods and Appl., Vol. 9, No. 2, pp. 93 – 133 (2003)

Weak first- and second-order numerical schemes for stochastic differential equations appearing in Lagrangian two-phase flow modeling

Jean-Pierre Minier[1], Eric Peirano[2] and Sergio Chibbaro[3]

[1] Electricité de France, MFTT, 6 Quati Watier 78400 France
[2] ADEME-Der, 500 Route des Lucioles 06560 Valbonne France
[3] Dipartimento di fisica and INFN, Università di Cagliari,
Cittadella Universitaria Monserrato CA, Italy
E-mail: Jean-Pierre.Minier@edf.fr, eric.peirano@ademe.fr, chibbaro@chi80bk.der.edf.fr

Abstract — Weak first- and second-order numerical schemes are developed to integrate the stochastic differential equations that arise in mean-field - pdf methods (Lagrangian stochastic approach) for modeling polydispersed turbulent two-phase flows. These equations present several challenges, the foremost being that the problem is characterized by the presence of different time scales that can lead to stiff equations, when the smallest time-scale is significantly less than the time-step of the simulation. The numerical issues have been detailed by Minier [Monte Carlo Meth. and Appl. **7** 295-310, (2000)] and the present paper proposes numerical schemes that satisfy these constraints. This point is really crucial for physical and engineering applications, where various limit cases can be present at the same time in different parts of the domain or at different times. In order to build up the algorithm, the analytical solutions to the equations are first carried out when the coefficients are constant. By freezing the coefficients in the analytical solutions, first and second order unconditionally stable weak schemes are developed. A prediction/correction method, which is shown to be consistent for the present stochastic model, is used to devise the second-order scheme. A complete numerical investigation is carried out to validate the schemes, having included also a comprehensive study of the different error sources. The final method is demonstrated to have the required stability, accuracy and efficiency.

1 Introduction

There is nowadays an increasing interest in modeling and simulating polydispersed turbulent two-phase flows of engineering significance [1]. In such flows, discrete particles are embedded in a fluid in turbulent motion. The complexity of these flows arises both from the multi-scale character of the problem and from the wide variety of physical phenomena involved (turbulence, particle dispersion, granular matter, combustion and so on).

Several methods can be used to model and simulate polydispersed turbulent two-phase flows. These approaches range from the microscopic level (exact local instantaneous equations) to the macroscopic level (mean field equations). They are often compared directly in the literature without specifying that there exists a hierarchy between them since they correspond to different levels of information [2]. For industrial applications, a good compromise between the level of information which is provided and the computational effort which is required, is obtained by the mean-field - pdf approach (or *Lagrangian stochastic approach*). In this approach, mean field equations (classical Reynolds stress models)

are derived for the fluid whereas particles are tracked individually by using a set of equations describing their dynamical behavior. In fact, real particles are replaced by stochastic particles where the time evolution of the variables of interest is described by stochastic differential equations (SDEs). In a weak sense, the use of SDEs is equivalent to a Monte-Carlo simulation of an underlying pdf [3], *i.e.* interest is not focused on the trajectories of the stochastic processes but on their joint law (pdf). Indeed, in most engineering applications, one is mainly interested in the expected values (statistics) of functionals of the variables of interest. In other words, the fluid is modeled at the macroscopic level whereas the dynamics of the particles are reproduced at a mesoscopic level (SDEs). The mesoscopic description is an intermediate level between the macroscopic description and the microscopic description. The mesoscopic description is rather natural when one attempts to address problems with complex physics [1]: for example, for reactive sprays, mean-field - pdf methods have the overwhelming advantage to represent exactly, for the particles, key phenomena such as combustion, convection and polydispersity without any approximation.

Numerical solutions to mean-field - pdf models require hybrid methods and are based on particle-mesh technique [4]. The mean-field equations are solved on a mesh by standard discretization techniques whereas the dynamics of the particles are obtained by time integration of the SDEs. From now on, let $\langle \mathbf{X} \rangle$ denote the set of mean fields representing the fluid, *i.e.* the mean velocity $\langle \mathbf{U}_f \rangle(t, \mathbf{x})$, the mean pressure $\langle P \rangle(t, \mathbf{x})$, the covariance matrix $\langle \mathbf{u}_f \mathbf{u}_f \rangle(t, \mathbf{x})$ and the mean energy dissipation rate, $\langle \epsilon \rangle(t, \mathbf{x})$ (the $\langle\ \rangle$ operator stands for the mathematical expectation). The SDEs reproducing the dynamics of the particles can be written as follows,

$$dZ_i(t) = A_i(t, \mathbf{Z}, \langle f(\mathbf{Z}) \rangle, \langle \mathbf{X} \rangle)\, dt + \sum_j B_{ij}(t, \mathbf{Z}, \langle f(\mathbf{Z}) \rangle, \langle \mathbf{X} \rangle)\, dW_j(t), \tag{1}$$

where $\mathbf{Z}$ is the state vector (the set of variables of interest) and $\mathbf{W}(t)$ is a vector of independent Wiener processes. $\mathbf{A}$ is the drift vector and $\mathbf{B}$ is the diffusion matrix. It is immediately seen that these equations are non-linear as the coefficients depend not only on the state vector but also on expected values of functions of $\mathbf{Z}$, not to the mention the dependence on the properties of the fluid (these equations are called Mac-Kean SDEs in the mathematical literature [5]). In particle-mesh methods, quantities such as $\langle f(\mathbf{Z}) \rangle$ are extracted from the particle data and evaluated at grid points . Therefore, the numerical integration of the SDEs requires the following steps:

(i) projection of $\langle f(\mathbf{Z}) \rangle$ and $\langle \mathbf{X} \rangle$ at particle positions to evaluate the coefficients $\mathbf{A}$ and $\mathbf{B}$.

(ii) Time integration of Eq. (1) with a suitable numerical scheme and (iii) averaging to compute the new values of the fields $\langle f(\mathbf{Z}) \rangle$ at grid points.

The purpose of this paper is to develop the second step, that is to provide efficient, stable and accurate numerical schemes in order to integrate the trajectories of the process. This implies two main difficulties.

(a) The first one arises from the nature of the stochastic models. SDEs do not obey the rules of classical differential calculus and one has to rely on the theory of stochastic processes [6]. In the present paper, Itô's calculus is adopted and therefore all SDEs are written in the *Itô sense*. For stochastic processes, several convergence modes are

possible, and as explained before, only weak convergence is under consideration. A discrete approximation $\mathbf{Y}_T$ (T stands for a given stopping time) converges in the weak sense with order p, if for any polynomial g, there exists a constant C, function of T, such that

$$|\langle g(\mathbf{Z}_T)\rangle - \langle g(\mathbf{Y}_T)\rangle| \leqslant C(T)\,\Delta t^p. \tag{2}$$

Due to the mathematical definition of Itô's integral, numerical schemes developed for SDE cannot be applied directly. Several work have already been performed for the integration of SDEs appearing in turbulent flow modeling [7, 8]. Here, these ideas are extended to a specific set of SDEs often encountered for modeling polydispersed turbulent two-phase flows. Our present objective is to develop weak numerical scheme that are second-order accurate in time, unconditionally stable but still explicit for the stochastic model we consider.

(b) The second difficulty is related to physical constraints. As suggested in [9], the general stochastic model used to simulate general dispersed two-phase flows contains several characteristic time-scales. When some of these time-scales become negligible (the system of SDEs is then stiff), various sub-systems of stochastic differential equations can be extracted. In other words, simplified stochastic models can be obtained from the general one. Our second objective is to put forward numerical schemes that can be still applicable, and that remain accurate, when the different time-scales go to zero. This corresponds to a practical concern. Indeed, in the numerical simulation of a complex flow, the time-scales may be negligible in some areas of the flows. We want nevertheless the general numerical scheme to reproduce the correct physical behaviour in these areas with the same numerical efficiency.

The original part of this work is just the numerical treatment of the multi-scale character of the problem in a physically sound manner. Indeed, an algorithm is presented that follows all the mathematical and physical constraints necessary to assure that in the scaling limit cases the expected equations are retrieved, with the fundamental property to be unconditionally stable, that allows us an arbitrary choice of the integration time step.

The paper is organized as follows. The stochastic differential system is presented in Section 2. The multi-scale specificity is discussed and analytical solutions are given for the system with constant coefficients. Then, in Section 3, a brief overview of the particle-mesh method, and its associated numerical errors, is presented. After that, the numerical schemes are derived. Numerical validations of the theoretical results of convergence are performed in Section 5. The paper closes with discussions and conclusions.

2 Analysis of the continuous system

In the present study, the equation system corresponds to non-reacting, incompressible fluid-particle flows, with no collisions between particles. Only heavy particles are under consideration, *i.e.* the density of the discrete particles is much greater than that of the fluid, $\rho_f \ll \rho_p$. Since the purpose of the study is neither the development of new models nor their numerical validation by comparison with experiments, the equation system is presented in a straight-forward manner without detailed information. All needed explanations can be found in Ref. [1].

2.1 Stochastic differential system

The fluid velocity seen is the velocity sampled by the discrete particles along their trajectories $\mathbf{x}_p(t)$. Extension of Kolmogorov theory [10] (for Lagrangian statistics of fluid elements) to discrete particles suggests that the acceleration of the fluid velocity seen $\mathbf{U}_s(t, \mathbf{x}_p(t))$ is a fast variable, if the process is observed at discrete time intervals dt which are large compared to the Kolmogorov time scale, τ, and small compared to the 'memory' (integral time scale) T_i of $\mathbf{U}_s$, *i.e.* $\tau \ll dt \ll T_i$. With this separation of scales, the fast variable can be eliminated by standard techniques (fast variable elimination [11]) and its influence is modeled by a stochastic differential equation. The remaining variables of interest are then position $\mathbf{x}_p$, particle velocity $\mathbf{U}_p$ and the fluid velocity seen $\mathbf{U}_s$ whose evolution in time can be described by the following stochastic differential system

$$\begin{cases} dx_{p,i} = U_{p,i}\, dt, \\ dU_{p,i} = \dfrac{1}{\tau_p}(U_{s,i} - U_{p,i})\, dt + \mathcal{A}_i\, dt, \\ dU_{s,i} = -\dfrac{1}{T_i} U_{s,i}\, dt + C_i\, dt + \displaystyle\sum_j \sigma_{ij}\, dW_j(t), \end{cases} \tag{3}$$

where τ_p is the particle relaxation time and $\mathcal{A}_i$ is an acceleration due to external force fields (gravity in most cases). σ_{ij} is the diffusion matrix and the meaning of C_i shall shortly be explained.

The particle relaxation time is defined as

$$\tau_p(d_p, \mathbf{U}_r) = \frac{\rho_p\, d_p}{\rho_f\, C_D |\mathbf{U}_\mathbf{r}|}, \tag{4}$$

where C_D, the drag coefficient, is a non-liner function of the particle Reynolds number $Re = |\mathbf{U}_\mathbf{r}|\, d_p/\nu_f$ (ν_f is the kinematic viscosity of the fluid, $\mathbf{U_r} = \mathbf{U_p} - \mathbf{U_s}$ the relative velocity and d_p the particle diameter). For heavy particles embedded in a turbulent flow undergoing gravity, it is possible to show that the acceleration $\mathcal{A}_i$ can be written

$$\mathcal{A}_i(t, \mathbf{x}_p) = -\frac{1}{\rho_p}\frac{\partial \langle P \rangle}{\partial x_i} + g_i, \tag{5}$$

where g_i is the gravitational acceleration.

Contrarily to Eqs (4) and (5), which can be considered as 'exact', the expressions presented now for the other parameters of system (3) can neither be considered as exact nor definitive. They simply correspond to the current level of knowledge. The memory of the fluid velocity seen is

$$T_i(t, \mathbf{x}_p, \langle \mathbf{U}_r \rangle) = T_f \left[1 + \beta_i \frac{3 |\langle \mathbf{U}_r \rangle|^2}{2k} \right]^{-1/2}, \tag{6}$$

where T_f, the integral time scale of the fluid, is defined as $T_f = C_\mu\, k/\langle \epsilon \rangle$. C_μ and β_i are constants (for β_i, the value of the constant depends on direction i). The dependence of T_i on time and position is due to the different fields entering Eq. (6) such as k and $\langle \epsilon \rangle$. The diffusion matrix is diagonal, but non-isotropic

$$\sigma_i(t, \mathbf{x}_p, \langle \mathbf{U}_r \rangle) = \langle \epsilon \rangle \left[C_0\, b_i\, \frac{\tilde{k}}{k} + \frac{2}{3}\left(b_i \frac{\tilde{k}}{k} - 1 \right) \right], \tag{7}$$

where C_0 is a constant, $b_i = T_f/T_i$ and

$$\tilde{k} = \frac{3}{2}\left(\sum_{i=1}^{3} b_i \langle u_{f,i}^2 \rangle\right) / \sum_{i=1}^{3} b_i. \tag{8}$$

Vector $\mathbf{C}$ is the sum of several terms

$$C_i(t, \mathbf{Z}, \langle f(\mathbf{Z}) \rangle) = \frac{\langle U_{s,i} \rangle}{T_i} - \frac{1}{\rho_f}\frac{\partial \langle P \rangle}{\partial x_i} + (\langle U_{p,j} \rangle - \langle U_{s,j} \rangle)\frac{\partial \langle U_{f,i} \rangle}{\partial x_j} + \frac{\chi}{\tau_p}(U_{p,i} - U_{s,i}), \tag{9}$$

where $\mathbf{Z} = (\mathbf{x}, \mathbf{U}_p, \mathbf{U}_s)$ is the state vector. The third and fourth terms on the right hand side of Eq. (9) have a clear physical meaning. The former expresses the influence of τ_p and g_i on the statistics of the fluid velocity seen and the latter accounts for two way-coupling. In this last term, χ is defined as $(\alpha_p\, \rho_p)/(\alpha_f\, \rho_p)$ where $\alpha_p(t, \mathbf{x}_p)$ is the local volume fraction of particles (α_f, the volume fraction of the fluid is computed by $\alpha_f = 1 - \alpha_p$).

2.2 Limit cases

Once again, system (3) has a physical meaning only in the case where $dt \ll T_i$ and $dt \ll \tau_p$. When this condition is not satisfied, it is possible to show that, in the *continuous sense* (time and all coefficients are continuous functions which can go to zero), the system converges towards several limit systems [9]. case 1: when $\tau_p \to 0$, the particles behave as fluid particles and one has

$$\text{system (3)} \xrightarrow[\tau_p \to 0]{} \begin{cases} dx_{p,i} = U_{p,i}\, dt \\ U_{p,i} = U_{s,i} \\ dU_{s,i} = -\dfrac{1}{T_i} U_{s,i}\, dt + C_i\, dt + \displaystyle\sum_j \sigma_{ij}\, dW_j(t) \end{cases} \tag{10}$$

We retrieve a known turbulent fluid PDF model [12]. This shows that our model is a coherent generalization of the fluid one, which can be recovered as limit case.

case 2: when $T_i \to 0$ and $\sigma_{ij} T_i \to cst$, the fluid velocity seen becomes a fast variable. It is then eliminated and one can write

$$\text{system (3)} \xrightarrow[T_i \to 0]{(\sigma_{ij} T_i \to cst)} \begin{cases} dx_{p,i} = U_{p,i}\, dt \\ dU_{p,i} = \dfrac{1}{\tau_p}(\langle U_{s,i} \rangle - U_{p,i})\, dt + \mathcal{A}_i\, dt + \displaystyle\sum_j \frac{\sigma_{ij} T_i}{\tau_p}\, dW_j(t) \end{cases} \tag{11}$$

In this case, the equations collapse in a Fokker-Planck model for large high-inertia particle.

case 3: When τ_p, $T_i \to 0$ and at the same time $\sigma_{ij} T_i \to cst$, the fluid velocity seen becomes a fast variable and the discrete particles behave as fluid particles. It can be shown that

$$\text{system (3)} \xrightarrow[\tau_p, T_i \to 0]{(\sigma_{ij} T_i \to cst)} dx_{p,i} = \langle U_{s,i} \rangle\, dt + \mathcal{A}_i\, dt + \sum_j (\sigma_{ij} T_i)\, dW_j(t). \tag{12}$$

We retrieve a pure diffusive behaviour, that is the equations of the *Brownian motion*. It is often used for large time lags simulations, being the case of $dt \gg T_i$, $dt \gg \tau_p$.

These three asymptotic cases reflect the multi-scale character of the problem. Three time scales are present: the 'observation' time scale, dt, and two physical time scales, the

particle relaxation time, τ_p, and the integral time scale of the fluid velocity seen, T_i. It is seen that, when these scales go to zero, a hierarchy of stochastic differential systems is obtained. Moreover, the elimination of the fast variables (the velocities $\mathbf{U}_p$ and $\mathbf{U}_s$) does not mean that these variables do not (physically) exist anymore: they are simply not mathematically defined. For example, in the case of Eq. (11), the fluid velocity seen becomes white noise (no memory, infinite variance).

case 4: at last, when $T_i \to 0$ with no condition on $\sigma_{ij}T_i$, the velocity of the fluid seen is no longer random and the system becomes deterministic. The flow is laminar and it can be proven that

$$\text{system (3)} \xrightarrow[T_i \to 0]{} \begin{cases} dx_{p,i} = U_{p,i}\, dt \\ dU_{p,i} = \dfrac{1}{\tau_p}(\langle U_{s,i}\rangle - U_{p,i})\, dt + \mathcal{A}_i\, dt \\ U_{s,i} = \langle U_{s,i}\rangle. \end{cases} \tag{13}$$

2.3 Analytical solutions

The construction of the numerical schemes is now slightly anticipated. Since the numerical methods are derived by freezing the coefficients on the integration intervals, the solutions to system (3), *with constant coefficients*, are now given.

By resorting to Itô's calculus, it can be shown that the analytical solutions are given by Eqs (B.2) to (B.4), see Table 1. For instance, for the fluid velocity seen, if one seeks a solution of the form $U_{s,i}(t) = H(t)\exp(-t/T_i)$, where $H(t)$ is a stochastic process, Itô's calculus gives

$$dH(t) = \exp(t/T_i)[C_i(\mathbf{x}_p)\, dt + \sum_j \sigma_{ij}(\mathbf{x}_p)\, dW_j(t)], \tag{14}$$

that is, by integration on a time interval $[t_0, t]$ ($\Delta t = t - t_0$),

$$\begin{aligned} U_{s,i}(t) = U_{s,i}(t_0)\exp(-\Delta t/T_i) + C_i(\mathbf{x}_p)\, T_i\,[1 - \exp(-\Delta t/T_i)] \\ + \sum_j \sigma_{ij}(\mathbf{x}_p)\exp(-t/T_i)\int_{t_0}^{t} \exp(s/T_i)\, dW_j(s). \end{aligned} \tag{15}$$

The previous expression is identical to Eq. (B.4) in Table 1. The analytical solutions for position, $\mathbf{x}_p(t)$, and velocity, $\mathbf{U}_p(t)$, given in Table 1, are obtained by a similar technique as the one used for the fluid velocity seen, $\mathbf{U}_s(t)$.

The three stochastic integrals, Eqs (B.5) to (B.7) in Table 1, only for the constant coefficient case, are Gaussian processes since they are stochastic integrals of deterministic functions [6]. These integrals can be re-written, by resorting to stochastic integration by parts, as the sum of simple stochastic integrals (see Appendix A.1), Eqs (B.8) to (B.10) in Table 1. By using Itô's calculus, the first two moments of each stochastic process (the stochastic integrals) can be calculated. The second order moments are displayed in Table 2 (the first order moments are, of course, all equal to zero). As a matter of fact, Table 2 gives the covariance matrix built from the stochastic integrals. The path to the final expressions is briefly explained in Appendix A.2.

Once again, the numerics are slightly anticipated and it is now explained how the stochastic integrals can be calculated (simulated). It has just been shown that these integrals are Gaussian processes whose means and variances are know (zero mean and covariance matrix given by Table 2). The vector composed by the nine stochastic integrals, Eqs

(B.5) to (B.7), is a vector of Gaussian centered random variables which can be computed by resorting to the simulation of a vector composed of independent normal Gaussian variables (zero mean and variance equal to one). This technique, which requires the Choleski decomposition of the covariance matrix, is displayed in Appendix B.

At last, let us check that the expressions of Table 1 and 2 are consistent with the limit cases given, *in the continuous sense*, in Section 3.2.

2.3.1 Limit case (i)

In limit case (i), where the discrete particles behave as fluid particles, the limit system is given by Eq. (10). When the coefficients are constant, the limit expressions are obtained from Table 1 and 2. Indeed, when $\tau_p \to 0$, Eq. (B.3) becomes

$$U_{p,i}(t) = U_{s,i}(t_0)\exp(-\Delta t/T_i) + C_i\, T_i \exp(-\Delta t/T_i) + \Gamma_i(t), \tag{16}$$

and for the stochastic integral $\Gamma_i(t)$, one has

$$\langle \Gamma_i^2(t) \rangle \xrightarrow[\tau_p \to 0]{} \frac{\breve{\sigma}_i^2\, T_i}{2}[1 - \exp(-2\Delta t/T_i)] = \langle \gamma_i^2(t) \rangle, \tag{17}$$

and also

$$\langle \Gamma_i(t)\, \gamma_i(t) \rangle \xrightarrow[\tau_p \to 0]{} \langle \gamma_i^2(t) \rangle. \tag{18}$$

The last two equations indicate that $\Gamma_i(t) \to \gamma_i(t)$ when $\tau_p \to 0$. By comparing Eq. (16) to Eq. (B.4), one has $U_{p,i}(t) = U_{s,i}(t)$ which is the consistent with the limit given in Section 3.2.

2.3.2 Limit case (ii)

In this case, the velocity of the fluid velocity seen is a fast variable which is eliminated. The results obtained in Table 1 and 2, when the coefficients of the system are constant, with $T_i \to 0$ and $\sigma_{ij}\, T_i \to cst$, give for the velocity of the discrete particles,

$$\begin{aligned} U_{p,i}(t) = U_{p,i}(t_0)\exp(-\Delta t/\tau_p) + [\langle U_{s,i}(t) \rangle + \mathcal{A}_i\, \tau_p][1 - \exp(-\Delta t/\tau_p)] \\ + \sqrt{\frac{\breve{\sigma}_i^2\, T_i^2}{2\tau_p}(1 - \exp(-2\Delta t/\tau_p)}\ \ \mathcal{G}_{p,i}, \end{aligned} \tag{19}$$

where $\mathcal{G}_{p,i}$ is $\mathcal{N}(0,1)$ vector (a vector composed of independent normal Gaussian random variables). It can be rapidly verified, by applying Itô's calculus, that Eq. (19) is the solution to system (11) when the coefficients are constant

2.3.3 Limit case (iii)

Here, both the fluid velocity seen and the velocity of the discrete particles become rapid variables. When $\tau_p \to 0$ and $T_i \to 0$ with $\sigma_{ij}\, T_i \to cst$, Eq. (B.2) becomes

$$x_{p,i}(t) = x_{p,i}(t_0) + [\langle U_{s,i}(t) \rangle + \mathcal{A}_i\, \tau_p]\, \Delta t + \sqrt{\breve{\sigma}_i^2\, T_i^2\, \Delta t}\ \ \mathcal{G}_{x,i}, \tag{20}$$

which is the solution to Eq. (12) when the coefficients are constant.

2.3.4 Limit case (iv)

When $T_i \to 0$ (with no condition on $\sigma_{ij}T_i$), the flow becomes laminar, which means that the system becomes deterministic, see Eq. (13). Once again, the results given by Table 1 and 2 are in agreement with Eq. (13). When $T_i \to 0$, Eqs (B.2) to (B.4) become

$$\begin{aligned}
&U_{s,i}(t) = \langle U_{s,i}(t)\rangle,\\
&U_{p,i}(t) = U_{p,i}(t_0)\exp(-\Delta t/\tau_p) + [\langle U_{s,i}\rangle + \mathcal{A}_i\,\tau_p][1-\exp(-\Delta t/\tau_p)],\\
&x_{p,i}(t) = x_{p,i}(t_0) + \tau_p[1-\exp(-\Delta t/\tau_p)]U_{p,i}(t_0) + [\langle U_{s,i}\rangle + \mathcal{A}_i\,\tau_p]\{\Delta t - \tau_p[1-\exp(-\Delta t/\tau_p)]\},
\end{aligned} \tag{21}$$

which is the analytical solution to system (13) when the coefficients are constant. Both the position and the velocity of the particles are increasing functions of time whose asymptotes are $[\langle U_{s,i}\rangle + \mathcal{A}_i\,\tau_p](\Delta t - \tau_p)$ (with a relaxation time of magnitude τ_p) and $\langle U_{s,i}\rangle + \mathcal{A}_i\,\tau_p$, respectively. In conclusion, in order to have a consistent and stable numerical scheme for the integration of such a type of SDEs, it is necessary to retain the exponential terms in the solution and all the stochastic integrals, even the *indirect* ones, must be explicitely calculated.

3 Derivation of the numerical method

The numerical solutions to system (3), with constant coefficients, are now known and it has been demonstrated that, from these solutions, the hierarchy of stochastic differential systems (limit cases) can be retrieved. Before presenting the derivation of the numerical schemes, let us first display the main steps of the particle-mesh method used in our computations. This will help us to define the constraint that the schemes must fulfill.

3.1 Particle-mesh method

In the present paper, all numerical computations are performed with the ESTET solver, developed by EDF. As mentioned in the introduction, in a particle-mesh method, particles are moving in a mesh where, at every node, the mean fields describing the fluid are known. The statistics extracted from the variables attached to the particles (which are needed to compute the coefficients of system (3)) are not calculated for each particle (this would cost too much CPU time) but are evaluated at each cell center following a given numerical scheme (averaging operator). These moments can then be evaluated for each particle by projection. This the principle of particle-mesh methods: exchange data between particle and mesh points. Once again, the expected value for functionals of the state vector are not computed directly for each particle but are evaluated at discrete points in space and then calculated for each particle by interpolation. The main advantage of such methods is of course the reduction of CPU time but these procedures have also some drawbacks: (i) additional numerical errors due to averaging and projection and (ii) each particle has to be located in the mesh.

Let us specify the different steps of the particle-mesh method implemented in the ESTET code and the associated numerical errors. Let $\{\mathbf{Z}^{(N)}\}$ denote the set of variables attached to the particles, $\{\mathbf{Z}^{[x]}\}$ the set of values of $\langle f(\mathbf{Z})\rangle$ at cell centers. Time is discretized with a uniform time step $\Delta t = t_{n+1} - t_n$ and space with a uniform mesh of cell size

Δx. The first step on the algorithm is to solve the PDEs (Partial Differential Equations) describing the fluid,

$$\langle \mathbf{X} \rangle(t_n) \text{ and } \mathbf{Z}^{[x]}(t_n) \xrightarrow{F} \langle \mathbf{X} \rangle(t_{n+1}).$$

This step is denoted by the F operator which simply means that from the set of fields known at time t_n, the set of fields at time t_{n+1} is computed. The F operator corresponds to a classical Navier-Stokes solver and it gives the evolution in time of the characteristics of the fluid (some particle properties are needed to compute source terms if two-way coupling is accounted for). The second step is to transfer particle properties and fluid properties (which are also needed to compute the coefficients of the stochastic differential system) from the mesh to the particles,

$$\mathbf{Z}^{[x]}(t_n) \text{ and } \langle \mathbf{X} \rangle(t_n) \xrightarrow{P} \mathbf{Z}^{(N)}(t_n) \text{ and } \langle \mathbf{X}^{(N)} \rangle(t_n),$$

where $\langle \mathbf{X}^{(N)} \rangle(t_n)$ represents the values of the fluid properties at particle locations. The P operator means that statistical moments known at mesh points (fluid) and cell centers (particles) are evaluated at particle locations. Then, the stochastic differential system is integrated in time,

$$\langle \mathbf{X}^{(N)} \rangle(t_n) \text{ and } \mathbf{Z}^{(N)}(t_n) \xrightarrow{T} \mathbf{Z}^{(N)}(t_{n+1}).$$

This step simulates the dynamics of the system under consideration. Finally, from the new computed set of variables, at particle locations, new statistical moments are evaluated at cell centers,

$$\mathbf{Z}^{(N)}(t_{n+1}) \xrightarrow{A} \mathbf{Z}^{[x]}(t_{n+1}),$$

and so on. In the present paper, the different numerical methods used to implement the A and P operators are not discussed (see [4] for further explanations) since the purpose of this work is to define operator T, *i.e.* to find a suitable weak numerical scheme for system (3).

Before explaining what a suitable weak numerical scheme should be, let us identify the different numerical errors which are inherent to particle-mesh methods. Some of these errors will be studied in the numerical validation of the scheme. The total error depends on three numerical parameters: Δt for time discretization, Δx for space discretization and N for the evaluation of statistical quantities by a finite set of particles. As explained by Xu and Pope [13], the total error (for $\langle f(\mathbf{Z}) \rangle$, the expected value of a functional of $\mathbf{Z}$) is, at time $t = T$,

$$\epsilon(T) = \langle f(\mathbf{Z}_T) \rangle - \{ f(\overline{\mathbf{Z}}_T) \}_{N,\Delta x}$$

where $\overline{\mathbf{Z}}_T$ (in the following $\mathbf{Z}(t)$ is often written $\mathbf{Z}_t$) is the approximation of $\mathbf{Z}_T$ after time integration (operator T) and $\{ \quad \}_{N,\Delta x}$ is the approximation of the expected value, for the definition of the expected value $\langle \quad \rangle$, that is of the mathematical expectation, see [5]. The total error, which is a random variable, can be decomposed as follows

$$\epsilon(T) = \epsilon_N(T) + \epsilon_{\Delta t}(T) + \epsilon_{\Delta x}(T) + \epsilon_\infty(T).$$

These numerical errors are:

(i) The **statistical** error:

$$\epsilon_N(T) = \langle \{ f(\overline{\mathbf{Z}}_T) \}_{N,\Delta x} \rangle - \{ f(\mathbf{Z}_T) \}_{N,\Delta x} \tag{22}$$

which is inherent to all Monte-Carlo methods. The statistical error is random and its asymptotic behavior is given by the central limit theorem.

(ii) The **bias**:

$$\epsilon_\infty(T) = \{f(\overline{\mathbf{Z}}_T)\}_{\infty,\Delta x} - \langle\{f(\overline{\mathbf{Z}}_T)\}_{N,\Delta x}\rangle. \tag{23}$$

The bias, which is a deterministic error, is the difference between the mean value of a quantity for a finite number of particles and the mean value for infinitely many particles, all other parameters being unchanged. This error is typical of non-linear stochastic differential equation.

(iii) The **time discretisation** error:

$$\epsilon_{\Delta t}(T) = \langle f(\mathbf{Z}_T)\rangle - \langle f(\overline{\mathbf{Z}}_T)\rangle \tag{24}$$

where $\langle f(\overline{\mathbf{Z}}_T)\rangle = \{f(\overline{\mathbf{Z}}_T)\}_{\infty,0}$. This deterministic error is due to the numerical integration in time of the stochastic differential system (T operator).

(iv) The **space discretisation** error:

$$\epsilon_{\Delta x}(T) = \langle f(\overline{\mathbf{Z}}_T)\rangle - \{f(\overline{\mathbf{Z}}_T)\}_{\infty,\Delta x}. \tag{25}$$

This deterministic error is due to the exchange of information between the mesh and the particles (A and P operators, and of course F for the fluid).

The main steps of the particle-mesh method implemented in the ESTET code have now been explained and the associated numerical errors have been identified. With this knowledge in mind, let us now define the specifications of the weak numerical scheme.

3.2 Constraints of the numerical schemes

In the particle-mesh method adopted here, the PDEs for the fluid are first solved and then the dynamics of the stochastic particles are computed. Thus, the scheme has to be *explicit*. Furthermore, the time step, which has to be the same for the integration of the PDEs and the SDEs, is imposed by stability conditions required by the F operator. This implies that, since there is no possibility to control the time step when integrating the SDEs, the numerical scheme has to be *unconditionally stable*. At last, since particle localization in a mesh is CPU demanding, the numerical scheme should minimize these operations. The first constraint is

(i) *The numerical scheme must be explicit, stable, of order* 2 *in time and the number of calls to particle localization has to be minimum.*

A practical to fulfill the stability condition is to base the scheme on the analytical solutions presented in Section 2.3. Indeed, the time step appears in decaying exponentials of the type $\exp(-\Delta t)$, which brings unconditional stability. Therefore, the second constraint is

(ii) *The numerical scheme must be consistent with the analytical solutions of the system when the coefficients are constant.*

(iii) *The numerical scheme must be consistent with all limit systems.*

For this delicate point, we can express from the discrete point of view the physical constraints that have been presented for continuous time before in section 2.2.

case 1: this concerns when $\tau_p \to 0$. In the discrete simulation, this corresponds to the situation where we have $\tau_p \ll \Delta t \ll T_i$. ¿From continuous point of view the particle velocity is eliminated from the set of governing equations since it relaxes to its driving force, the velocity of the fluid seen, $U_p(t) \to U_s(t)$. In the numerical simulation, this means that by putting τ_p to zero, we should have at each time step k that $U_p(k\Delta t) = U_s(k\Delta t)$.

case 2: this is obtained when $T_i \to 0$. In that case, the velocity of the fluid seen is a deterministic function rather than a random one. In the numerical simulation, this means that putting T_i to zero, we should have at each time step k that $U_s(k\Delta t) = \langle U_s \rangle (k\Delta t, x_p(k\Delta t))$.

case 3: when $\tau_p \to 0$ as well as $T_i \to 0$ and $\sigma_{ij} T_i \to cst$ we have $T_i, \tau_p \ll \Delta t$. In that case, both U_s and U_p behave as fast variables. In the numerical simulation, this corresponds to the situation where we have $T_i, \tau_p \ll \Delta t$. Then, we expect to find that at each time step we have

$$U_p(k\Delta t) = U_s(k\Delta t) \tag{26}$$

$$U_s(k\Delta t) = \langle U_s \rangle (k\Delta t, x_p(k\Delta t)) + \sqrt{\sigma_{ij}^2 T_i}(k\Delta t, x_p(k\Delta t))\, e \tag{27}$$

with $e = N(0,1)$ is a random term sampled independently for each particle and at each time step in a normalized Gaussian distribution.

case 4: when $T_i \to 0$. ¿From the continuous point of view, the velocity of the fluid seen U_s will behave as a fast variable and a near white-noise term. In the numerical simulation, the velocity of the fluid seen U_s does not, of course, behave strictly-speaking as white-noise function (its variance is not infinite!), but this continuous limit corresponds to the situation where we have $T_L^* \ll \Delta t \ll \tau_p$. We expect the numerical simulation to yield that at, each time step, we have

$$U_s(k\Delta t) = \langle U_s \rangle (k\Delta t, x_p(k\Delta t)) + \sqrt{\sigma_{ij}^2 T_i}(k\Delta t, x_p(k\Delta t))\, e \tag{28}$$

where $e = N(0,1)$ is a Gaussian random term as in case 3.

The construction of the scheme on the analytical solutions should also ensure a sound physical treatment of the multi-scale character of the problem. Indeed, it has been demonstrated that from the analytical solutions given in Section 2.3, all limit cases can be retrieved. The last constraint on the scheme is then

The specifications of the numerical schemes are now known and each of them has been motivated in the frame of the particle-mesh method implemented in the ESTET code. The derivation of the numerical schemes can now begin.

4 Numerical schemes

4.1 Weak first-order scheme

The derivation of the weak first order scheme is rather straight forward since the analytical solutions of system (3) with constant coefficients have been evaluated. Indeed, the Euler scheme (which is a weak scheme of order 1 [14]) is simply obtained by freezing the

coefficients at the beginning of the time intervals $\Delta t = [t_n, t_{n+1}]$. Let Z_i^n and Z_i^{n+1} be the approximated values of Z_i at time t_n and t_{n+1}. The Euler scheme is then simply written by using the results of Tables 1 and 2 as shown in Table 3. From now on, this scheme is referred to as sch1. This scheme fulfills all criteria listed in Section 3.2, except, of course, the order of convergence in time.

As far as the consistency with all limit systems is concerned, some precisions must be given. Here, it has to be understood that the limit systems are presented in the *discrete sense*. The observation time scale dt has now become the time step Δt. The physical time scale τ_p and T_i do not go to zero, as in the continuous sense, but their values, depending on the history of the particles, can be smaller or greater than Δt.

For example, in limit case (ii), the condition $T_i \to 0$ must be understood as $T_i \ll \Delta t$. By Taylor expansion on Eq. (B.3), Eq. (16) is obtained (where of course Δt is the time step). When $\tau_p \to 0$, in the continuous limit case, the fluid velocity becomes a fast variable which is eliminated. In the discrete case, the velocity of the fluid seen is simply observed at a time intervals which are greater than its memory. For the present scheme, Eq. (B.4), with $1 \ll \Delta t/T_i$, gives

$$U_{s,i}^{n+1} = \langle U_{s,i}^n \rangle + \sqrt{\frac{[\check{\sigma}_i^n]^2\, T_i^n}{2}}\ \mathcal{G}_{1,i}, \tag{29}$$

This result is physically sound. Indeed, when a fluctuating physical process (random variable) is observed at time steps which are greater that its memory, the expected behavior is Gaussian.

Moreover, in limit case (iii), that is when $1 \ll \Delta t/T_i$ and $1 \ll \Delta t/\tau_p$ (discrete case), one obtains for the velocity of the particles, Eqs. (B.3), and for the fluid velocity seen, Eq. (B.4),

$$\begin{aligned} U_{p,i}^{n+1} &= \langle U_{s,i}^n \rangle + \mathcal{A}_i^n\, \tau_p^n + \sqrt{\frac{[\check{\sigma}_i^n]^2}{2}}\frac{T_i^n}{T_i^n + \tau_p^n}(\sqrt{T_i^n}\, \mathcal{G}_{s,i} + \sqrt{\tau_p^n}\, \mathcal{G}_{p,i}), \\ U_{s,i}^{n+1} &= \langle U_{s,i}^n \rangle + \sqrt{\frac{[\check{\sigma}_i^n]^2\, T_i^n}{2}}\ \mathcal{G}_{1,i}. \end{aligned} \tag{30}$$

It is seen, once again, that the particle velocity, $U_{p,i}(t)$, and the fluid velocity seen, $U_{s,i}(t)$, which were eliminated in the continuous case, do not disappear. They become Gaussian random variables, a result which is physically sound since these two random variables are observed at time steps which are greater than their respective memories.

4.2 Weak second order scheme

4.2.1 Property of the system

The diffusion matrix of system (3) has a singular property, that have a crucial importance here [15]. From Eq. (7), it can be noticed that σ_{ij} depends only on time, position and the mean value of the relative velocity. Therefore, the only variable of the state vector whom σ_{ij} is a function is $\mathbf{x}_p$. Therefore, the diffusion matrix has the following singular property

$$\sum_k \sum_l \sigma_{kl} \frac{\partial \sigma_{ij}}{\partial x_k} = 0, \quad \forall\, (i,j,k,l). \tag{31}$$

4.2.2 General method

Let us consider, for a moment, the following stochastic differential equation

$$dX_i(t) = A_i(\mathbf{X}(t))\,dt + \sum_j B_{ij}(\mathbf{X}(t))\,dW_j(t)$$

where $\mathbf{A}$ is the drift vector and $\mathbf{B}$ is the diffusion matrix. If $\mathbf{B}$ verifies the *commutativity condition*, it can be shown that, for example by stochastic Taylor expansions [14], a prediction-correction scheme of the type

$$\begin{aligned} \tilde{X}_i^{n+1} &= X_i^n + A_i^n\,dt + \sum_j B_{ij}^n\,\Delta W_j, \\ X_i^{n+1} &= X_i^n + \frac{1}{2}\left(A_i^n + \tilde{A}_i^{n+1}\right)dt + \sum_j \frac{1}{2}\left(B_{ij}^n + \tilde{B}_{ij}^{n+1}\right)\Delta W_j, \end{aligned} \tag{32}$$

is a weak second order scheme ($\tilde{A}_i^{n+1} = A_i(\tilde{\mathbf{X}}^{n+1})$ and $\tilde{B}_{ij}^{n+1} = B_{ij}(\tilde{\mathbf{X}}^{n+1})$). This result is true, one again, only when the commutativity condition is verified. If not, other terms are needed in order to obtain a weak second order scheme, see for example Talay [16].

The idea is now to built from Eq. (32) and derive a weak second order scheme for system (3). As in Eq. (32), the Euler scheme (first order scheme sch1) is going to be used as a prediction step. The remaining task consists in finding a suitable correction step which enforces the three conditions listed in Section 3.2.

4.2.3 Implementation of the scheme

The main idea for the implementation of the correction step is to start from the analytical solutions to system (3) when the coefficients are constant and apply the same idea as in Eq. (32) and consider that the acceleration terms vary linearly with time.

Before the implementation of the numerical scheme, let us specify the notation which is in use. As in Section 4.1, Z_i^n and Z_i^{n+1} stand for the approximated values of Z_i at time t_n and t_{n+1}, respectively. Therefore, Z_i^{n+1} is the corrected value whereas the predicted value is denoted $\tilde{Z}_i^{n+1}$, *i.e.* the value of Z_i predicted by the Euler scheme. The predicted velocities are $\tilde{U}_{p,i}^{n+1}$ and $\tilde{U}_{s,i}^{n+1}$ and the values of the fields taken at $(t_{n+1},\, \mathbf{x}_p^{n+1})$ are denoted, for example, $\langle U_{s,i}^{n+1}\rangle$ or $\langle P^{n+1}\rangle$. The predicted time scales are referred to as $\tilde{T}_i^{n+1}$ and $\tilde{\tau}_p{}^{n+1}$ and the predicted diffusion matrix is designated by $\tilde{\sigma}_{ij}^{n+1}$.

As far as the computation of the fields 'attached' to the particles are concerned, it is worth emphasizing that none of them are computed at $(t_{n+1},\, \mathbf{x}_p^{n+1})$, because the scheme would become implicit. All fields which characterize the fluid, such as the mean pressure field, are taken at $(t_{n+1},\, \mathbf{x}_p^{n+1})$, but fields such as the expected value of the fluid velocity seen are computed from the predicted velocities. For example, one has

$$C_i(t_{n+1},\, \mathbf{x}_p^{n+1}) = C_i^{n+1} = \frac{1}{\tilde{T}_i^{n+1}}\langle U_{s,i}^{n+1}\rangle + \Pi_i(\langle\tilde{\mathbf{U}}_s^{n+1}\rangle, \langle\tilde{\mathbf{U}}_p^{n+1}\rangle, \langle\mathbf{U}_f^{n+1}\rangle, \langle P^{n+1}\rangle).$$

The analytical solution to system (3) when the coefficients are constant is, for the fluid velocity seen, by applying the rules of Itô's calculus

$$U_{s,i}(t) = U_{s,i}(t_0)\,\exp(-\Delta t/T_i) + \int_{t_0}^{t} C_i(s, \mathbf{x}_p)\exp[(s-t)/T_i]\,ds + \gamma_i(t). \tag{33}$$

Let us suppose, as mentioned previously, that the acceleration $C_i(s, \mathbf{x}_p)$ varies linearly on the integration interval $[t_0, t]$, that is

$$C_i(s, \mathbf{x}_p(s)) = C_i(t_0, \mathbf{x}_p(t_0)) + \frac{1}{\Delta t}[C_i(t, \mathbf{x}_p(t)) - C_i(t_0, \mathbf{x}_p(t_0))](s - t_0). \tag{34}$$

By direct integration, one can write

$$U_{s,i}(t) = U_{s,i}(t_0)\, \exp(-\Delta t/T_i) + [T_i\, C_i(t_0, \mathbf{x}_p(t_0))]\, A(\Delta t, T_i) + [T_i\, C_i(t, \mathbf{x}_p(t))]\, B(\Delta t, T_i) + \gamma_i(t),$$

where the functions $A(\Delta t, X)$ and $B(\Delta t, X)$ are given by

$$A(\Delta t, X) = -\exp(-\Delta t/X) + \left[\frac{1 - \exp(-\Delta t/X)}{\Delta t/X}\right],$$
$$B(\Delta t, X) = 1 - \left[\frac{1 - \exp(-\Delta t/X)}{\Delta t/X}\right].$$

By direct application of the ideas presented in Section 4.2.2, it is proposed to write

$$\begin{aligned} U_{s,i}^{n+1} =& \frac{1}{2}\, U_{s,i}^n\, \exp(-\Delta t/T_i^n) + \frac{1}{2}\, U_{s,i}^n\, \exp(-\Delta t/\tilde{T}_i^{n+1}) \\ &+ A(\Delta t,\, T_i^n)\, [T_i^n C_i^n] + B(\Delta t,\, \tilde{T}_i^{n+1})\, [\tilde{T}_i^{n+1} \tilde{C}_i^{n+1}] + \tilde{\gamma}_i^{n+1}, \end{aligned}$$

where the stochastic integral is simulated by ($\mathcal{G}_{1,i}$ is the $\mathcal{N}(0,1)$ random variable used in the simulation of γ_i^n in the Euler scheme, see Table 3)

$$\tilde{\gamma}_i^{n+1} = \sqrt{[\sigma_i^*]^2 \frac{\tilde{T}_i^{n+1}}{2}[1 - \exp(-2\Delta t/\tilde{T}_i^{n+1})]}\ \ \mathcal{G}_{1,i},$$

and where σ_i^* is defined by

$$\sigma_i^* = \left[A(2\,\Delta t,\, \tilde{T}_i^{n+1}) \sqrt{\sum_j (\sigma_{ij}^n)^2} + B(2\,\Delta t,\, \tilde{T}_i^{n+1}) \sqrt{\sum_j (\tilde{\sigma}_{ij}^{n+1})^2}\right] \ \left[1 - \exp(-2\,\Delta t/\tilde{T}_i^{n+1})\right]^{-1}.$$

Here, it can already be seen by simple stochastic calculus (stochastic Taylor expansions) that the expression proposed for the diffusion matrix in the correction step, σ_i^*, enforces that the scheme is of second order in time.

In the case of the velocity of the particles, the same approach followed for the fluid velocity seen is adopted. Let us start from the exact solution with constant coefficients for $U_{p,i}(t)$. By resorting to the rules of Itô's calculus, one can write

$$U_{p,i}(t) = U_{p,i}(t_0) \exp(-\Delta t/\tau_p) + \frac{1}{\tau_p} \exp(-\Delta t/\tau_p) \int_{t_0}^{t} \exp(s/\tau_p)[U_{s,i}(s) + \tau_p\, \mathcal{A}_i(s, \mathbf{x}_p)]\, ds,$$

and by inserting Eq. (33) in the previous equation, one has

$$\begin{aligned} U_{p,i}(t) =&\ U_{p,i}(t_0) \exp(-\Delta t/\tau_p) + U_{s,i}(t_0)\, \theta_i[\exp(-\Delta t/T_i) - \exp(-\Delta t/\tau_p)] + \Gamma_i(t) \\ &+ \frac{1}{\tau_p} \exp(-t/\tau_p) \int_{t_0}^{t} \exp(s/\tau_p) \left[\exp(-s/T_i) \int_{t_0}^{s} C_i(u, \mathbf{x}_p)\, \exp(u/T_i)\, du + \tau_p\, \mathcal{A}_i(s, \mathbf{x}_p)\right] ds. \end{aligned} \tag{35}$$

Two deterministic integrals must be treated in Eq. (35). A multiple one, involving $C_i(t,\mathbf{x}_p)$ and a simple one with the acceleration term $\mathcal{A}_i(t,\mathbf{x}_p)$. Both integrals are handled as done previously for the fluid velocity seen, that is, it is assumed that both accelerations vary linearly on the integration interval, see for example Eq. (34) for $C_i(t,\mathbf{x}_p)$. By integration by parts on both integrals, one finds after some derivations

$$\begin{aligned} U_{p,i}(t) = {} & U_{p,i}(t_0)\exp(-\Delta t/\tau_p) + U_{s,i}(t_0)\,\theta_i[\exp(-\Delta t/T_i) - \exp(-\Delta t/\tau_p)] \\ & + [T_i\,C_i(t_0,\mathbf{x}_p(t_0))]\,A_c(\tau_p,T_i) + [T_i\,C_i(t,\mathbf{x}_p(t))]\,B_c(\tau_p,T_i) \\ & + [\tau_p\,\mathcal{A}_i(t_0,\mathbf{x}_p(t_0))]\,A(\Delta t,\tau_p) + [\tau_p\,\mathcal{A}_i(t,\mathbf{x}_p(t))]\,B(\Delta t,\tau_p) + \Gamma_i(t), \end{aligned}$$

where the functions $C_c(X,Y)$, $A_c(X,Y)$ and $B_c(X,Y)$ are given by

$$\begin{aligned} C_c(X,Y) &= \frac{Y}{Y-X}\,[\exp(-\Delta t/Y) - \exp(-\Delta t/X)], \\ A_c(X,Y) &= -\exp(-\Delta t/X) + \frac{X+Y}{\Delta t}[1-\exp(-\Delta t/X)] - \left(1+\frac{Y}{\Delta t}\right)\,C_c(X,Y), \\ B_c(X,Y) &= 1 - \frac{X+Y}{\Delta t}[1-\exp(-\Delta t/X)] + \frac{Y}{\Delta t}\,C_c(X,Y). \end{aligned}$$

In analogy with the results of Section 4.2.2, the following correction step is proposed,

$$\begin{aligned} U_{p,i}^{n+1} = {} & \frac{1}{2}\,U_{p,i}^n\,\exp(-\Delta t/\tau_p^n) + \frac{1}{2}\,U_{p,i}^n\,\exp(-\Delta t/\tilde{\tau}_p^{n+1}) \\ & + \frac{1}{2}\,U_{s,i}^n\,C_c(\tau_p^n,\,T_i^n) + \frac{1}{2}\,U_{s,i}^n\,C_c(\tilde{\tau}_p^{n+1},\,\tilde{T}_i^{n+1}) \\ & + A_c(\tau_p^n,\,T_i^n)\,[T_i^n C_i^n] + B_c(\tilde{\tau}_p^{n+1},\,\tilde{T}_i^{n+1})\,[\tilde{T}_i^{n+1} C_i^{n+1}] \\ & + A(\Delta t,\tau_p^n)[\tau_p^n\,\mathcal{A}_i^n] + B(\Delta t,\tilde{\tau}_p^{n+1})[\tilde{\tau}_p^{n+1}\,\mathcal{A}_i^{n+1}] + \tilde{\Gamma}_i^{n+1}. \end{aligned} \tag{35}$$

For the simulation of the stochastic integral, one has (where $\mathcal{G}_{2,i}$ is the $\mathcal{N}(0,1)$ random variable used in the simulation of Γ_i^n in the Euler scheme, see Table 3)

$$\tilde{\Gamma}_i^{n+1} = \frac{\langle\tilde{\Gamma}_i^{n+1}\tilde{\gamma}_i^{n+1}\rangle}{\langle(\tilde{\gamma}_i^{n+1})^2\rangle}\,\tilde{\gamma}_i^{n+1} + \sqrt{\langle(\tilde{\Gamma}_i^{n+1})^2\rangle - \frac{[\langle\tilde{\Gamma}_i^{n+1}\tilde{\gamma}_i^{n+1}\rangle]^2}{\langle(\tilde{\gamma}_i^{n+1})^2\rangle}}\,\mathcal{G}_{2,i},$$

where the second order moments $\langle\tilde{\Gamma}_i^{n+1}\tilde{\gamma}_i^{n+1}\rangle$ and $\langle(\tilde{\Gamma}_i^{n+1})^2\rangle$ are computed from Eqs. (B.12) and (B.14), respectively, by inserting the suitable time scales and diffusion matrix, that is τ_p^n, $\tilde{T}_i^{n+1}$ and σ_i^*. This completes the weak second order scheme.

It can be shown, by stochastic Taylor expansion [14] or by verifying the conditions given by Talay [16], that the present scheme is a weak order scheme of order 2 in time for system (3). It is worth emphasizing that no correction is done on position, $\mathbf{x}_p$, since the prediction is already of order 2. This property is in line with the constraint stated in Section 3.2, that is, the numerical scheme should minimize the procedures where particles must be located in a mesh (which is done every time the particles are moved, *i.e.* when a new value of $\mathbf{x}_p$ is computed). The complete scheme is summarized in Table 4.

4.2.4 Limit cases

In limit case (i), when $1 \ll \Delta t/\tau_p$, one has $A_c(\tau_p,T_i) \to A(\Delta t,T_i)$, $B_c(\tau_p,T_i) \to B(\Delta t,T_i)$ and $C_c(\tau_p,T_i) \to \exp(-\Delta t/T_i)$. For the stochastic integral, one can show, as done in

Section 2.3.4 that $\tilde{\Gamma}_i^{n+1} \to \tilde{\gamma}_i^{n+1}$. By inserting these results in Eq. (35), one can write

$$U_{p,i}^{n+1} = U_{s,i}^{n+1}, \tag{36}$$

which is consistent with Eq. (10). In addition, Eq. (36) is a second order scheme for $U_{p,i}(t)$, and therefore the scheme remains of order 2 in limit case (i).

When $1 \ll \Delta t/T_i$ and $\sigma_{ij}\, T_i \to cst$ (limit case (ii)), one has $A_c(\tau_p, T_i) \to A(\Delta t, \tau_p)$ and $B_c(\tau_p, T_i) \to B(\Delta t, \tau_p)$, which gives for the numerical correction of the velocity of the particles

$$\begin{aligned} U_{p,i}^{n+1} = \frac{1}{2}\, U_{p,i}^{n}\, \exp(-\Delta t/\tau_p^n) + \frac{1}{2}\, U_{p,i}^{n}\, \exp(-\Delta t/\tilde{\tau}_p^{n+1}) \\ + A(\Delta t, \tau_p^n)[\langle U_{s,i}^n \rangle + \tau_p^n\, \mathcal{A}_i^n] + B(\Delta t, \tilde{\tau}_p^{n+1})[\langle \tilde{U}_{s,i}^{n+1} \rangle + \tilde{\tau}_p^{n+1}\, \mathcal{A}_i^{n+1}] + \tilde{\Gamma}_i^{n+1}. \end{aligned} \tag{37}$$

For the simulation of the stochastic integral, one can prove by looking at the limit values (when $1 \ll \Delta t/T_i$ and $\sigma_{ij}\, T_i \to cst$) in Eqs. (B.11), (B.12) and (B.14) that (here $\mathcal{G}'_{p,i}$ is a $\mathcal{N}(0,1)$ random variable)

$$\tilde{\Gamma}_i^{n+1} \to \sqrt{\frac{[\sigma_i^*\, \tilde{T}_i^{n+1}]^2}{2\, \tilde{\tau}_p^{n+1}}[1 - \exp(-2\Delta t/\tilde{\tau}_p^{n+1})]}\ \mathcal{G}'_{p,i},$$

which is in accordance with Eq. (19). Unfortunately, it can be established, again by Taylor stochastic expansion, that the scheme is not of second order in time for system (11), but of first order. This is due to the treatment of the correction step for the stochastic integral $\Gamma_i(t)$, a problem which is not solved yet and left outside the scope of the present paper. As far as the fluid velocity seen is concerned, one has

$$U_{s,i}^{n+1} = \langle U_{s,i}^{n+1} \rangle + \sqrt{\frac{[\sigma_i^*]^2\, \tilde{T}_i^{n+1}}{2}}\ \mathcal{G}_{1,i}, \tag{38}$$

which is in line with the previous results, see Section 2.3.2. This scheme is of second order, but the whole scheme is not. Indeed, as mentioned above, the scheme is only of first order for the velocity of the particle and therefore of first order for the position of the particles.

When both the fluid velocity seen and the velocity of the particles become fast variables (limit case (iii)), that is when $1 \ll \Delta t/T_i$, $1 \ll \Delta t/\tau_p$ and $\sigma_{ij}\, T_i \to cst$, one can write for the velocity of the particle, for example from Eq. (37) with $1 \ll \Delta t/\tau_p$,

$$U_{p,i}^{n+1} = \langle \tilde{U}_{s,i}^{n+1} \rangle + \tilde{\tau}_p^{n+1}\, \mathcal{A}_i^{n+1} + \sqrt{\frac{[\sigma_i^*\, \tilde{T}_i^{n+1}]^2}{2\, \tilde{\tau}_p^{n+1}}}\ \mathcal{G}'_{p,i}.$$

For the fluid velocity seen, Eq. (38) is unchanged. These results are consistent with the expressions of Section 2.3.3. In limit case (iii), the numerical scheme for the position of the particles is equivalent to the Euler scheme written previously and is of first order in time.

When the flow becomes laminar, that is when $T_i \to 0$ with no condition on the product $\sigma_{ij}\, T_i$, one has the following limits: $A(\Delta t, T_i) \to 0$, $B(\Delta t, T_i) \to 1$ and $\gamma_i(t) \to 0$, which gives for the fluid velocity seen,

$$U_{s,i}^{n+1} = \langle \tilde{U}_{s,i}^{n+1} \rangle.$$

For velocity of the particles, the coefficient have the following limits: $A_c(\tau_p, T_i) \to A(\Delta t, \tau_p)$, $B_c(\tau_p, T_i) \to B(\Delta t, \tau_p)$ and $C_c(\tau_p, T_i) \to 0$ which gives together with the limit $\Gamma_i(t) \to 0$,

$$U_{p,i}^{n+1} = \frac{1}{2} U_{p,i}^n \exp(-\Delta t/\tau_p^n) + \frac{1}{2} U_{p,i}^n \exp(-\Delta t/\tilde{\tau}_p^{n+1}) + A(\Delta t, \tau_p^n)[\langle U_{s,i}^n \rangle + \tau_p^n \mathcal{A}_i^n] + B(\Delta t, \tilde{\tau}_p^{n+1})[\langle \tilde{U}_{s,i}^{n+1} \rangle + \tilde{\tau}_p^{n+1} \mathcal{A}_i^{n+1}].$$

It can rapidly be shown, by regular Taylor expansion, that this scheme, together with the prediction step (Euler scheme sch1) is a second order scheme for system (13).

In summary, a weak-second order scheme for system (3) has been derived. This scheme satisfies all conditions listed in Section 3.2, except for the second order convergence condition in limit cases (ii) and (iii). In the former case, this imperfection is bearable since the situation $T \ll \Delta t$ does not occur very often in practice. In the latter case, the first order convergence is inherent to the spirit of the scheme, that is a single step to compute position $\mathbf{x}_p$ (in order to minimize the number of particle localizations in the algorithm).

5 Numerical studies

It has been explained previously in Section 3.1 that particle-mesh methods generate several numerical errors. A statistical error which is inherent to the Monte-Carlo method and a deterministic error which is the sum of three distinct terms (the bias, the time discretisation error and the spatial discretisation error). In the present paper, where interest in only focused on the study of weak numerical schemes for system (3), only the time discretisation error is of interest (among the deterministic errors) in order to study the speed of convergence.

In the following, ideal cases will be chosen where there is no exchange between the mesh and the particles, and therefore no spatial discretisation error, *i.e.* $\epsilon_{\Delta x}(T) = 0$, see Eq. (25). In addition, the ideal systems will be linear, which implies the elimination of the bias in the numerical procedure, *i.e.* $\epsilon_\infty(T) = 0$, see Eq. (23). In such cases, the statistical and the time discretisation errors can be studied. These errors are defined by Eqs (22) and (24), respectively. In our particular case, one has for the approximation of the mathematical expectation

$$\{f(\overline{\mathbf{Z}}_T)\}_{N,\Delta x} = \{f(\overline{\mathbf{Z}}_T)\}_N = \frac{1}{N} \sum_{i=1}^N f(\overline{\mathbf{Z}}_T^i),$$

where $\overline{\mathbf{Z}}_T^i$ represents the value of $\overline{\mathbf{Z}}_t$ at time $t = T$ for trajectory i. Therefore, the statistical error, see Eq. (22), can be written

$$\epsilon_N(T) = \langle f(\overline{\mathbf{Z}}_T) \rangle - \frac{1}{N} \sum_{i=1}^N f(\overline{\mathbf{Z}}_T^i).$$

The central limit theorem tells us that, for a sufficiently large number of trajectories, this random variable converges, in the weak sense, towards a Gaussian random variable, that is ($\mathcal{G}$ is a $\mathcal{N}(0,1)$ random variable)

$$\epsilon_N(T) \xrightarrow[N \to +\infty]{\text{in law}} \frac{\sigma[f(\overline{\mathbf{Z}}_T)]}{\sqrt{N}} \mathcal{G}$$

where $\sigma[f(\overline{\mathbf{Z}}_T)]$ is the r.m.s. value of $f(\overline{\mathbf{Z}}_T)$.

In summary, the total error is, in our particular case, the sum of two errors: the statistical error and the time discretisation error. From the previous considerations, one can state that the total error is a random variable which, for a sufficiently large number of trajectories, becomes Gaussian. Its mean and r.m.s. value are given by,

$$\langle \epsilon(T) \rangle = \epsilon_{\Delta t}(T), \quad \sigma[\epsilon(T)] = \frac{\sigma[f(\overline{\mathbf{Z}}_T)]}{\sqrt{N}}.$$

The time discretisation error is deterministic and consequently one has, for the variance operator, $\mathrm{var}[\epsilon(T)] = \mathrm{var}[\epsilon_N(T)]$. For a weak numerical scheme of order of convergence p, one has

$$|\epsilon_{\Delta t}(T)| = C(T)\,(\Delta t)^p + O(\Delta t)^{p+1}, \tag{39}$$

where $C(T)$ is a constant which depends on the problem and stopping time T.

5.1 Limit cases and statistical error

Here, it is recalled that one of the constraint required in Section 3.2, was that the scheme should be identical to the analytical solution for constant coefficients. In order to study the statistical error, without bothering about the (time) discretisation one, let us study an ideal case with constant coefficients. This case will also be used to check that the numerical schemes are consistent with the limit cases.

5.1.1 Preliminary study

Let us consider an isotropic case where $C_i(t, \mathbf{x}_p) = 0$, $\mathcal{A}_i(t, \mathbf{x}_p) = 0$ and where the initial conditions are given by $x_p(0) = U_p(0) = U_s(0) = 0$. In this case, the system,

$$\begin{cases} dx_p = U_p\, dt \\ dU_p = \dfrac{1}{\tau_p}(U_s - U_p)\, dt \\ dU_s = -\dfrac{1}{T} U_s\, dt + \sigma\, dW(t), \end{cases} \tag{40}$$

admits $x_p(t) = \Omega(t)$, $U_p(t) = \Gamma(t)$ and $U_s(t) = \gamma(t)$ as a solution. These random variables are Gaussian and they have zero mean and known variances, see Table 2. As a matter of fact, all second order moments (variances) are increasing functions of time with the following asymptotes

$$\begin{aligned} \langle \Omega^2(t) \rangle &\xrightarrow[t\to\infty]{} \sigma^2\theta^2 (T - \tau_p)^2\, t + B, \\ \langle \Gamma^2(t) \rangle &\xrightarrow[t\to\infty]{} \frac{\sigma^2 T}{2} \frac{T}{T + \tau_p}, \\ \langle \gamma^2(t) \rangle &\xrightarrow[t\to\infty]{} \frac{\sigma^2 T}{2}, \end{aligned} \tag{41}$$

where the constant B is defined as

$$B = \frac{\sigma^2\theta^2}{2(T + \tau_p)} \left(T^3 + \tau_p^3 - 4(T - \tau_p)^2 (T + \tau_p) - 4\frac{T^2\tau_p^2}{T + \tau_p} \right).$$

In the stationary case, that is as time goes to infinity, the velocities become stationary processes, and one can verify the well-known Tchen formulas which give a relation between the energy of the particles, the energy of the fluid seen and the velocity covariance,

$$\frac{\langle U_p^2(t)\rangle}{\langle U_s^2(t)\rangle} = \frac{T}{T+\tau_p} \quad \text{and} \quad \langle U_p(t)\, U_s(t)\rangle = \langle U_p^2(t)\rangle.$$

The equality, in the stationary case, between the energy of the particles and the velocity covariance, can be obtained easily by noticing that

$$\langle \Gamma(t)\, \gamma(t)\rangle \xrightarrow[t\to\infty]{} \frac{\sigma^2 T}{2}\frac{T}{T+\tau_p}.$$

5.1.2 Limit cases

Let us now verify that the two (sch1 and sch2) numerical schemes, which have been implemented in the ESTET software, fulfill two of the constraints given in Section 3.2, that is (i) the numerical scheme gives the exact solution when the coefficients are constant and (ii) the numerical scheme is consistent in the limit cases, see Sections 2.3.1 to 2.3.4. To do so, the system presented in the previous Section is studied. The values taken by the (constant) coefficients in the different cases are presented in Table 7. It can be seen that the time step is constant and therefore the separation of scales is obtained by varying the coefficients: in this numerical example, it is considered that there is a separation of scales when the ratio between the smallest one and the greatest one is roughly 10^{-2}.

In practice, the code is modified in order to simulate the trajectories in a domain which can be considered as infinite (the particles never reach the boundaries so that boundary-condition effects can be avoided). It is also possible to adjust the value on the mean fluid velocity, $\langle \mathbf{U}_f \rangle$ (this will be necessary in the laminar case, when $T \to 0$). Here, since the purpose of the simulations is not the study of the statistical error, only 6000 trajectories are simulated (actually 2000 since the code is three-dimensional and the problem is isotropic) and there will be some noise in the numerical solutions. As a matter of fact, it is observed that there is no difference between the numerical solutions given by the sch1 and sch2 schemes. This not surprising since, with constant coefficients, the correction step of sch2 is rigorously the Euler scheme, sch1. This will be the case in all simulations presented in this subsection and this will not be recalled. The results are now displayed for the second order moments, the first order moment are generally omitted since the solutions are Gaussian random variables of zero mean.

In the general case, Fig. 1, when $\Delta t \ll \tau_p$ and $\Delta t \ll T$, it can be seen that both schemes are in agreement with the analytical solutions. One can verify that the limit values for $\langle U_p^2(t)\rangle$ and $\langle U_s^2(t)\rangle$ are correct, that is $\sigma^2 T/2 = 10$ and $(\sigma^2 T/2)/[T/(T+\tau_p)] = 6.67$, respectively, see Eq. (41). The results are also in line with the Tchen formulas, $\langle U_p^2(t)\rangle/\langle U_s^2(t)\rangle = T/(T+\tau_p) = 6.67/10 = 2/3$ and $\langle U_p(t)\, U_s(t)\rangle = \langle U_p^2(t)\rangle$. Furthermore, the limit behavior of $\langle x_p^2(t)\rangle$ is correct since the slope of the asymptote is $(\sigma\, T)^2 = 4$.

For limit case (i), Fig. 2, the fluid velocity seen and the particle velocity become identical (all second order moments are equal) . The limit values for $\langle U_p^2(t)\rangle$ and $\langle U_s^2(t)\rangle$ are $\sigma^2 T/2 = 5$, and for $\langle x_p^2(t)\rangle$ the slope of the asymptote is $(\sigma\, T)^2 = 1$. The Tchen formulas are verified, $\langle U_p^2(t)\rangle/\langle U_s^2(t)\rangle = T/(T+\tau_p) \simeq 1$ and $\langle U_p(t)\, U_s(t)\rangle = \langle U_p^2(t)\rangle$.

For limit case (ii), Fig. 3, the fluid velocity seen becomes a fast variable, that is, in the discrete case, $U_s(t)$ is a Gaussian random variable of zero mean, see Fig. 6, and variance

$\sigma^2 T/2 = 5$. The asymptote for $\langle U_p^2(t)\rangle$ is $(\sigma\, T)^2/2\tau_p = 5.10^{-4}$, which is in agreement with Eq. (41). The slope of the asymptote for $\langle x_p^2(t)\rangle$ is $(\sigma\, T)^2 = 10^{-4}$. As far as the Tchen formulas are concerned, it is verified that $\langle U_p^2(t)\rangle/\langle U_s^2(t)\rangle = T/(T+\tau_p) \simeq 10^{-4}$ and $\langle U_p(t)\, U_s(t)\rangle = \langle U_p^2(t)\rangle$.

In the diffusive regime, limit case (iii), Fig. 4, both the fluid velocity seen, $U_s(t)$, and the particle velocity, $U_p(t)$, become fast variables, which in the discrete case gives two Gaussian random variables of zero mean, see for example Fig 6 for $U_p(t)$, and of variances $\sigma^2 T/2 = 5$ and $(\sigma\, T)^2/[T/(T+\tau_p))] = 1.67$, respectively, see for example Eq. (30). For $\langle x_p^2(t)\rangle$, the slope of the asymptote is indeed given by $(\sigma\, T)^2 = 10^{-4}$. The Tchen formulas are also verified, $T/(T+\tau_p) = 1/3$.

At last, in the laminar case, limit case (iv), Fig. 5 shows a laminar flow with an imposed mean fluid velocity, $\langle U_s(t)\rangle = 1\ m/s$. It is seen that the asymptotes obtained for $\langle U_p(t)\rangle$ and $\langle x_p(t)\rangle$ are in agreement with the results derived in Section 2.3.4, $\langle U_p(t)\rangle \to \langle U_s(t)\rangle$ and $\langle x_p(t)\rangle \to \langle x_p(t)\rangle = t - 0.1$ when $t \to \infty$. Furthermore, the numerical behavior of the variances, for example for $x_p(t)$, shows that the dynamics of the particle is deterministic (similar results were obtained for $\langle U_p^2(t)\rangle$ and $\langle U_s^2(t)\rangle$).

Finally, as far as the first order moments are concerned, Fig. 6 shows that the numerical values obtained are in line with the zero mean result. For example, for the 95% confidence interval, one has, in the general case, an approximation of U_s centered in 0 and of radius $1.96\,\sigma[U_s]/\sqrt{N} \simeq 0.08$ ($\sigma[U_s]$ is the r.m.s. value of U_s). In the limit case (i), the 95% confidence interval for $\langle U_p\rangle$ gives $1.96\,\sigma[U_p]/\sqrt{N} \simeq 0.06$ ($\sigma[U_p]$ is the r.m.s. value for U_p) which is consistent with Fig. 6.

It has now been verified that the numerical schemes implemented in ESTET are consistent with the analytical solutions and the limit cases. Let us now study the statistical error.

5.1.3 Statistical error

Here, the study is based on simulations of the system (with constant coefficients) used in Section 5.1.1, and this is done in the general case, Table 7. It is recalled that, when the coefficients are constant, there is no discretisation error since the numerical scheme corresponds exactly to the analytical solution.

The limit behavior (for a sufficiently large number of trajectories) of the statistical error is given by the central limit theorem, that is the random variable, $\epsilon_N(T)$, converges (in law) towards a Gaussian random variable of zero mean and known variance. In practical simulations, it is not always possible to satisfy the hypothesis of the central limit theorem as, for example, one has to resort to pseudo-random number generators and it can not be guarantees that all simulated trajectories are independent. Still, it is well known, from the theory of propagation of chaos, that the results of convergence on $\epsilon_N(T)$ hold. Let us verify this result numerically.

Let us suppose that the results from the theory of propagation of chaos are not known. The variance of the statistical error, for any quantity $f(Z_T)$, is now under investigation, that is

$$\sigma^2[\epsilon_N(T)] = \langle\ (\epsilon_N(T) - \langle\epsilon_N(T)\rangle)^2\ \rangle,$$

which is equivalent to study the variance of the estimator, $\{\quad\}_N$, (at a fixed time $t = T$)

$$\mathcal{V}_N[f(Z_T)] = \langle\ (\{f(Z_T)\}_N - \langle\{f(Z_T)\}_N\rangle)^2\ \rangle.$$

Here, $\overline{Z}_T = Z_T$ since there is no time discretisation error. The variance is estimated by performing a sufficiently large number M of simulations so that $\mathcal{V}_N$ becomes roughly independent of M. These simulations, with different values for N, are going to give $\mathcal{V}_N[f(Z_T)]$ as a function of N. This will be performed for the first and second order moments, $f(Z_T) = Z_T$ and $f(Z_T) = Z_T^2$, respectively. For $f(Z_T) = Z_T$, the quantity to evaluate is

$$\mathcal{V}_N[Z_T] = \frac{1}{M}\sum_{i=1}^{M}\left(\{Z_T\}_N^i - \frac{1}{M}\sum_{i=1}^{M}\{Z_T\}_N^i\right)^2,$$

and it must be shown that $\sqrt{\mathcal{V}_N[Z_T]} \simeq \sigma(Z_T)/\sqrt{N}$ where $\sigma(Z_T)$ is the r.m.s. value of Z_T. For $f(Z_T) = Z_T^2$, the expression

$$\mathcal{V}_N[Z_T^2] = \frac{1}{M}\sum_{i=1}^{M}\left(\{Z_T^2\}_N^i - \frac{1}{M}\sum_{i=1}^{M}\{Z_T^2\}_N^i\right)^2,$$

is computed to show that the expected behavior $\sqrt{\mathcal{V}_N[Z_T^2]} \simeq \sigma(Z_T^2)/\sqrt{N}$ ($\sigma(Z_T^2)$ is the r.m.s. value of Z_T^2) is obtained. The exact values for $\sigma(Z_T)$ when $Z_T = x_p(T)$, $U_p(T)$, $U_s(T)$ are easily obtained in our particular case, that is $\sqrt{\langle\Omega^2(T)\rangle}$, $\sqrt{\langle\Gamma^2(T)\rangle}$ and $\sqrt{\langle\gamma^2(T)\rangle}$, respectively. Since Z_T is a Gaussian random variable (it is a stochastic integral of a deterministic function), one has $\langle Z_T^4\rangle = 3\langle Z_T^2\rangle$ and therefore

$$\sigma(Z_T^2) = \sqrt{2}\,[\sigma(Z_T)]^2.$$

The presumed analytical expressions of $\mathcal{V}_N$ (for Z_T et Z_T^2) are now known. Numerical tests have shown that, on average, a good approximation of $\mathcal{V}_N$ is obtained for $M = 200$. This can be seen in Fig. 7 for $Z_T = x_p(T)$ and $Z_T = U_p(T)$ as an example. This value can be confirmed by resorting to the Bikelis theorem. Shortly, this theorem states that, for a given random variable Z_T, it is possible to specify the number of trajectories N which are necessary to approximate $\langle Z_T\rangle$ with a given precision ϵ and a confidence interval given by δ, that is $P(|\langle Z_T\rangle - \{Z_T\}_N| \leqslant \epsilon) \geq 1 - \delta$. For example, for $\mathcal{V}_N$ with $Z_T = x_p(T)$, one obtains $M \simeq 150$ for $\delta = 0.05$ and $\epsilon = 10^{-4}$. At last, it has also been checked that the numerical results do not depend on the time step, see Fig. 8 for $Z_T = x_p(T)$.

Based on the previous observations, M simulations are performed for different values of N with $t = T$ as final time. The results for the first and second order moments of $x_p(T)$, $U_p(T)$, $U_s(T)$ show the expected behavior, Fig. 11, that is a convergence rate for the variance of the statistical error in $1/N$.

5.2 Discretisation error

The study of the discretisation error has to be performed in a numerical case where the influence of the statistical error is negligible, in other words one has to make sure that the error is almost deterministic. In the simulations, the following approximation is made

$$\langle\epsilon(T)\rangle = \epsilon_{\Delta t}(T) \simeq \{\epsilon(T)\}_M, \tag{42}$$

which means that, as in the study of the statistical error, M simulations with N trajectories each are performed. The previous approximation induces a numerical error $\epsilon_M(T)$ defined by

$$\epsilon_M(T) = \langle\epsilon(T)\rangle - \{\epsilon(T)\}_M,$$

and from the central limit theorem (or the theory of propagation of chaos as mentioned above), this random variable converges, for M and N sufficiently large, towards a Gaussian random variable

$$\epsilon_M(T) \xrightarrow[M\to+\infty]{\text{in law}} \frac{\sigma[\epsilon(T)]}{\sqrt{M}}\,\mathcal{G} \xrightarrow[M,N\to+\infty]{\text{in law}} \frac{\sigma[f(Z_T)]}{\sqrt{M\times N}}\,\mathcal{G},$$

where $\mathcal{G}$ is a $\mathcal{N}(0,1)$ random variable (here the central limit theorem has been applied twice, first to $\epsilon_M(T)$ and then to $\epsilon_N(T)$). A confidence interval, for example 95 %, can then be given

$$P\left(|\epsilon_\Delta(T) - \{\epsilon(T)\}_M| \leqslant 1.96\,\frac{\sigma[f(Z_T)]}{\sqrt{M\times N}}\right) = 0.95.$$

Here, the Bikelis theorem can be applied to estimate the value of M which is necessary to approximate $\epsilon_{\Delta t}(T)$ with a given precision in a chosen confidence interval. It is now obvious that a good approximation of the discretisation error can only be obtained in cases where N and M are large and $\sigma[f(Z_T)]$ is small. Before going on with the numerical tests, let us look for a system with non-constant coefficients and known analytical solutions (so that quantities such as $\langle f(Z_T)\rangle$ can be computed).

5.2.1 Analytical solutions

Let us suppose that the coefficients depend on time only and look for analytical solutions to the following system

$$\begin{cases} dx_p = U_p\,dt, \\ dU_p = -\beta(t)(U_p - U_s), \\ dU_s = -\alpha(t)U_s\,dt + \sigma(t)\,dW(t). \end{cases} \tag{43}$$

The exact solutions to system (43) are given by

$$\begin{aligned} x_p(t) &= x_p(t_0) + \int_{t_0}^{t} U_p(s)\,ds, \\ U_p(t) &= U_p(t_0)\exp[-G(t)] + \exp[-G(t)]\int_{t_0}^{t}\exp[G(t)]\,\beta(s)\,U_s(s)\,ds, \\ U_s(t) &= U_s(t_0)\exp[-F(t)] + \exp[-F(t)]\int_{t_0}^{t}\exp[F(t)]\,\sigma(s)\,dW(s), \end{aligned}$$

where the function $F(t)$ and $G(t)$ are given by

$$F(t) = \int_{t_0}^{t}\alpha(s)\,ds \quad \text{and} \quad G(t) = \int_{t_0}^{t}\beta(s)\,ds. \tag{44}$$

Consequently, the functions $\alpha(t)$, $\beta(t)$, and $\sigma(t)$ must be chosen in such way so that the moments of order 1 and 2, which will used for the study of the numerical error, can be calculated explicitly. Some constraints must be, however, satisfied so that the system has a physical meaning (positiveness of coefficients, smoothness, ...). As already suggested by Haworth and Pope [7], in a study of a simpler system, the basic idea is to take for $\alpha(t)$ and

$\beta(t)$ functions whose primitives are logarithms. This property eliminates the exponentials. Let us write

$$\alpha(t) = \frac{a}{\alpha_0\, t + 1} \quad \text{and} \quad \alpha(t) = \frac{b}{\alpha_0\, t + 1},$$

where a, b and α_0 take real positive values and therefore

$$F(t) = \left[\ln\left(\alpha_0\, s + 1\right)^k\right]_{t_0}^t \quad \text{and} \quad G(t) = \left[\ln\left(\alpha_0\, s + 1\right)^n\right]_{t_0}^t,$$

where $k = a/\alpha_0$ and $n = b/\alpha_0$. For the diffusion coefficient, an expression which allows control (in time) and exact integration, is proposed, that is

$$\sigma(t) = \sigma_0(\alpha_0\, t + 1)^p$$

where σ_0 takes real positive values and p is real.

The moments of order 1 and 2 can now be calculated. The same initial conditions that were used for the study of the numerical error, are chosen (zero initial conditions on all variables at time $t_0 = 0$). This implies that all first order moments are equal to zero, see Table 5 where the analytical solutions for $x_p(t)$, $U_p(t)$ and $U_s(t)$ are given. The moments of order 2 are given in Tables 5 and 6. These quantities are now used for validation of the theoretical order of convergence (in time) of the weak numerical schemes sch1 and sch2.

5.2.2 Numerical study

The numerical value of the parameters of system (43) chosen in the simulations of the general case and the limit cases are displayed in Table 8. These values are essentially chosen (i) to respect the constraints of separation of scales in the different cases and (2) to make sure that the system remains stochastic, that is the diffusion coefficient is of the same order of magnitude as the drift term.

It is recalled that, for a sufficiently large number of particles N and simulations M, the discretisation error can be approximated by Eq. (42) and in practical simulations

$$\langle \epsilon(T) \rangle = \langle f(\overline{Z}_T) \rangle - \{\{f(\overline{Z}_T)\}_N\}_M, \tag{45}$$

where the convergence, in time, of $\langle \epsilon(T) \rangle$ is given by Eq. (39). As mentioned above, the numerical approximation of the discretisation error creates a statistical error $\epsilon_M(T)$ whose influence must be controlled. In fact, the problem is to find a time interval $[\Delta t_{min},\, \Delta t_{max}]$ where Δt_{min} has to specified so that the statistical error is negligible. For Δt_{max}, one has to make sure that this value does not exceed the time step at which the higher order terms, $(p+1)$, can become larger that the low order ones, p, see Eq. (39).

The values of the time step intervals, Δt_{min}, were limited essentially by the capacity of the computer (SUN Ultra 10 with 250 MBytes of memory). For the sch1 scheme, it was not difficult to study two decades whereas, for the sch2 scheme only a decade could be obtained. For the first order scheme, $N = 3.10^4$ trajectories, $M = 100$ simulations, a final time $T = 2.4\, s$ and the time steps $\Delta t = [0.4,\, 0.2,\, 0.1,\, 0.05]$ were used. For the second order scheme, of course more trajectories and simulations were necessary, $N = 9.10^5$ and $M = 200$, and a final time $T = 3.2\, s$ with larger time steps $\Delta t = [0.8,\, 0.4,\, 0.2,\, 0.1]$ were chosen. The final time for sch2 was different from that of sch1 only to match an integer number with the largest time step, $\Delta t = 0.8$. These values are summarized in Table 9.

Several alternatives were tested to decrease the value of Δt_{min}, apart from the increase of N and M. The final time T was changed (in order to increase $C(T)$) and the values of the parameters were modified (in order to decrease $\sigma[f(Z_T)]$). None of these strategies were successful. Indeed, in the general case, the dependence of $C(T)$ as a function of the parameters of the problem is not known, and it is difficult, except in simplified cases, to get estimates [17]. In fact, the only efficient method would have been a variance reduction technique. This issue, which is strongly problem dependent, has not been treated here.

Fig. 12 displays the results of the simulations in the general case (the error is normalized with its maximum value). It is shown that both schemes have the expected order of convergence. For limit case (i), Fig. 13 shows once again that the expected order of convergence is obtained. When the fluid velocity seen becomes a fast variable, limit case (ii), the second order scheme becomes, as mentioned in Section 4.2.4, a first order scheme, see Fig. 9. The same phenomenon is observed in limit case (iii), when both the fluid velocity seen and the particle velocity become fast variables, Fig. 10. In this last case, the statistical error on position $x_p(t)$ is unfortunately important.

6 Conclusions

Weak first- and second-order numerical schemes have been developed to integrate the set of stochastic differential equations which represent the result of a PDF approach to the problem of turbulence polydispersed two-phase flows. These equations have several intrinsical challenges. Since they are stochastic, they do not obey the rules of classical differential calculus, making a completely different approach necessary to achieve an algorithm consistent with the equations and with the desired order of integration. Moreover, they show a multi-scale character, that is different time scales are present in the equations more than the discrete time step Δt, they are the response time of the fluid and of the particles, respectively T_i and τ_p. The fact that one or both of them can take much smaller values than the integration time step leads, in this asymptotic limit, to singular equations, with specified physical behaviour. This has a major consequence, an algorithm which is not unconditionally stable would require a related small integration time step, with the net result of dramatically diminished efficiency. These properties of the system have caused an original and particular approach to achieve our aim.

The analytical solutions of the system in the case of constant coefficients are carried out, and all the stochastic integrals that arise from the integration are explicitly evaluated in order to satisfy the asymptotic limits. Starting from the analytical solution an unconditionally stable weak first-order Euler scheme has been developed. Then, a stable weak second-order scheme has been built up adopting a two-stage predictor-corrector strategy. The predictor stage is represented by the Euler scheme, while for the corrector stage all the terms are calculated explicitly. The use of analytical solutions as starting point and the exhaustive treatment of the limit cases have assured the requested stability and efficiency. It is worth emphasizing a point that can be misleading. This kind of algorithm is proved to have the requested features for the particular set of stochastic equations dealt with in this paper, but it is not straightforwardly applicable in a different situation, where problems of consistency can arise.

The numerical method has been implemented and verified with a comprehensive study, that includes a number of numerical simulations, worked out in various situations, to isolate

all the interesting features. Particularly, the behaviour in all the limit cases is presented and the different forms of errors are described. Four different errors can be defined, the statistical error, bias, the time discretisation and the space discretisation, among them the characteristics of statistical and discretisation ones are studied extensively. The numerical results indicate that the algorithms presented are quite satisfactory, as far as convergence, stability, accuracy and also asymptotic behaviour are concerned.

Acknowledgments

We would like to thank Prof. Denis Talay for numerous valuable and fruitful discussions during the development of the present work.

References

[1] J-P. Minier and E. Peirano. The pdf approach to polydispersed turbulent two-phase flows. *Physics Reports*, 352(1–3):1–214, 2001.

[2] E. Peirano and J-P. Minier. A probabilistic formalism and hierarchy of models for polydispersed turbulent two-phase flows. *Phys. Rev. E.*, 65(046301), 2002.

[3] J. Pozorski and J-P. Minier. Probability density function modelling of dispersed two-phase turbulent flows. *Physical Review E*, 59(1):855–863, 1998.

[4] R. W. Hockney and J. W. Eastwood. *Computer simulations using particles.* Institute of Physics Publishing, Bristol and Philadelphia, 1988.

[5] L. Arnold. *Stochastic Differential Equations: Theory and Applications.* Wiley, New-York, 1974.

[6] F. C. Klebaner. *Introduction to stochastic calculus with applications.* Imperial College Press, London, 1999.

[7] D. C. Haworth and S. B. Pope. A second-order Monte-Carlo method for the solution of the Itô stochastic differential equation. *Stochastic Analysis and Applications*, 4(2):151–186, 1986.

[8] S. B. Pope. Particle method for turbulent flows: integration of stochastic model equations. *J. Comput. Phys.*, 117:332–349, 1995.

[9] J-P. Minier. Probabilistic approach to turbulent two-phase flows modelling and simulation: theoretical and numerical issues. *Monte Carlo Methods and Appl.*, 7(3–4):295–310, 2000.

[10] A. S. Monin and A. M. Yaglom. *Statistical Fluid Mechanics.* MIT Press, Cambridge, Mass, 1975.

[11] H. Haken. Synergetics: an overview. *Rep. Prog. Phys.*, 52:515–533, 1989.

[12] S. B. Pope. Lagrangian pdf methods for turbulent reactive flows. *Annu. Rev. Fluid Mech.*, 26:23–63, 1994.

[13] Xu J. and Pope S.B. Assessment of numerical accurary of pdf/monte carlo methods for turbulent reacting flows. *J. Comput. Phys.*, 152:192, 1999.

[14] P.E. Kloeden and E. Platen. *Numerical solution of stochastic differential equations.* Springer-Verlag, Berlin, 1992.

[15] J-P. Minier, R. Cao, and S. B. Pope. Comment on the article "an effective particle tracking scheme on structured/unstructured grids in hybrid finite volume/pdf monte carlo methods" by li and modest. *J. Compt. Phys.*, 186:356–358, 2003.

[16] D. Talay. *Simulation of Stochastic Differential Equation, in* Probabilistic Methods in Applied Physics. Springer-Verlag, Berlin, 1995. P. Kree and W. Wedig.

[17] D. Talay. Probabilistic models for non-linear partial differential equations and numerical applications. In D. Talay and L. Tubaro, editors, *Lecture Notes in Mathematics 1627*, pages 148–196. CIME Summer School, Springer-Verlag, 1996.

A Calculus of the stochastic integrals

Here, it is explained how the stochastic integrals, *appearing in the analytical solutions of the equation system with constant coefficients*, can be re-arranged (by stochastic integration by parts), to yield the covariance matrix.

A.1 Integration by parts

Let $X(t)$ and $Y(t)$ be two diffusion processes. One can show that (see for example Klebaner [6]), in the Itô sense,

$$X(t)Y(t) - X(t_0)Y(t_0) = \int_{t_0}^{t} X(s)\,dY(s) + \int_{t_0}^{t} Y(s)\,dX(s) + [X,Y](t),$$

where $[X,Y](t)$ is the quadratic covariation of $X(t)$ and $Y(t)$ on $[t_0,t]$. In the case where one of the processes is deterministic, $[X,Y](t) = 0$. In the frame of our study, where the integrated variable is always a deterministic function, one can therefore apply integration by parts as in classical differential calculus.

In fact, in the analytical solutions of the equation system with constant coefficients, one encounters multiple stochastic integrals of the type

$$I = \int_{t_0}^{t} \exp(-s/a) \left(\int_{t_0}^{s} \exp(s'/b)\,dW(s') \right) ds, \tag{A.1}$$

where $(a,b) \in \mathbb{R}^{+2}$. By setting

$$\begin{aligned} F(s) &= \int_{t_0}^{s} \exp(s'/b)\,dW(s') \implies dF(s) = \exp(s/b)\,dW(s), \\ dG(s) &= \exp(-s/a) \implies G(s) = -a\,\exp(-s/a)\,ds, \end{aligned}$$

and applying integration by parts, one obtains

$$I = -a\,\exp(-t/a) \int_{t_0}^{t} \exp(s/b)\,dW(s) + a \int_{t_0}^{t} \exp(-s/a)\,\exp(s/b)\,dW(s). \tag{A.2}$$

Therefore, by stochastic integration by parts, the multiple integral given by Eq. (A.1) can be written as the sum of two simple stochastic integrals, Eq. (A.2).

A.2 Derivation of the covariance matrix

By using the results of the previous subsection and the main properties of the Itô integral, that is, linearity, the zero mean property,

$$\langle \int_{t_0}^{t} X(s)\,dW(s) \rangle = 0,$$

and the isommetry property,

$$\langle \int_{t_0}^{t_1} X(s)\,dW(s) \int_{t_2}^{t_3} Y(s)\,dW(s) \rangle = \int_{t_2}^{t_1} \langle X(s)Y(s) \rangle\,ds,$$

with $t_0 < t_2 < t_1 < t_3$, the covariance matrix formed by the stochastic integrals of Table 1, Eqs (B.5) to (B.7), can be evaluated. From the zero mean property, it follows that the first order moments are equal to zero. For the second order moments (covariance matrix), the previous properties give the following equality

$$\left\langle \left(\sum_m g_m(t) \int_{t_0}^{t} f_m(s)\, dW(s) \right)^2 \right\rangle = \sum_m g_m^2(t) \int_{t_0}^{t} f_m^2(s)\, ds + 2 \sum_{m<k} g_m(t)\, g_k(t) \int_{t_0}^{t} f_m(s)\, f_k(s)\, ds. \tag{A.3}$$

where $g_{im}(t)$ and $f_{im}(t)$ are deterministic functions of time. Eq. (A.3) allows us to derive the covariance matrix, Eqs (B.11) to (B.14), from Eqs (B.8) to (B.10).

B Simulation of a Gaussian vector

Let $\mathbf{X} = (X_1, \ldots, X_d)$ be a Gaussian vector defined by a zero mean and a covariance matrix $C_{ij} = \langle X_i X_j \rangle$. For all positive symmetric matrix (such as C_{ij}), there exists a (low or high) triangular matrix P_{ij} which verifies

$$\mathbf{C} = \mathbf{P}\mathbf{P}^t \implies C_{ij} = \sum_{k=1}^{d} P_{ik} P_{jk}.$$

$\mathbf{P}$ is given by the Choleski algorithm (here for the low triangular matrix)

$$\begin{aligned}
P_{i1} &= \frac{C_{i1}}{\sqrt{(C_{11})}}, \quad 1 \leqslant i \leqslant d \\
P_{ii} &= \left(C_{ii} - \sum_{j=1}^{i-1} P_{ij} \right)^{1/2}, \quad 1 < i \leqslant d \\
P_{ij} &= \frac{1}{P_{jj}} \left(C_{ij} - \sum_{k=1}^{j-1} P_{ik} P_{jk} \right), \quad 1 < j < i \leqslant d \\
P_{ij} &= 0, \quad i < j \leqslant d.
\end{aligned}$$

Let $\mathbf{G} = (G_1, \ldots, G_d)$ be a vector composed of independent $\mathcal{N}(0,1)$ Gaussian random variables, then it can be shown that the vector $\mathbf{Y} = \mathbf{P}\mathbf{G}$ is a Gaussian vector of zero mean and whose covariance matrix is $\mathbf{C} = \mathbf{P}\mathbf{P}^t$. Therefore, $\mathbf{X}$ and $\mathbf{Y}$ are identical, that is,

$$\mathbf{X} = \mathbf{P}\mathbf{G} \implies X_i = \sum_{k=1}^{d} P_{ik} G_k. \tag{B.1}$$

Eq. (B.1) shows how the stochastic integrals, obtained in the analytical solutions of the system with constant coefficients, can be simulated.

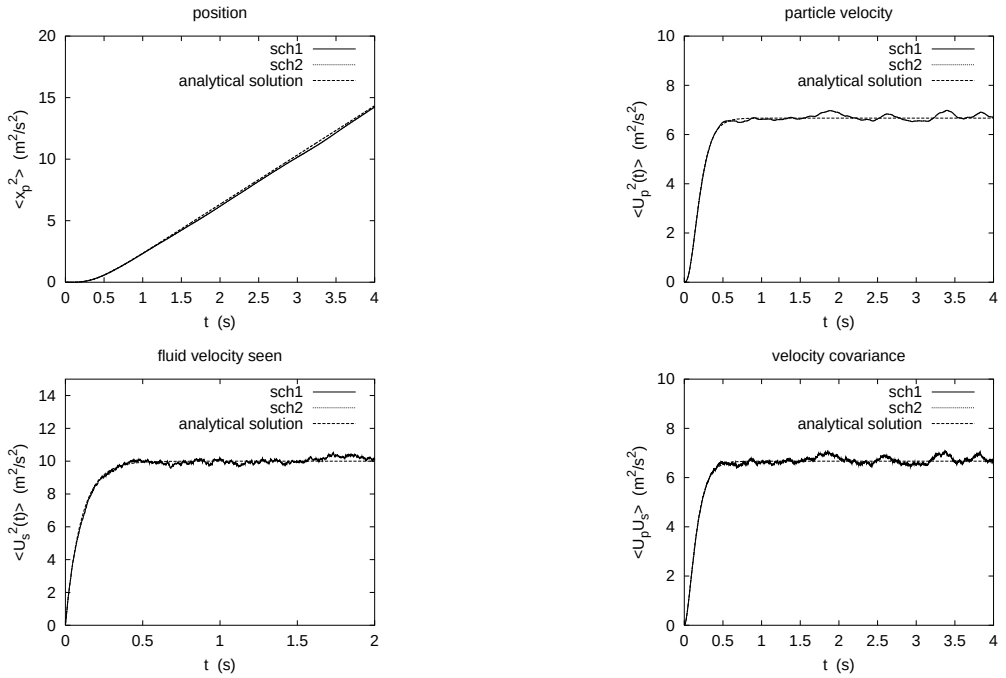

Figure 1: Numerical simulation with $N = 6000$ for system (40). General case: $\Delta t \ll T, \tau_p$ with $\Delta t = 10^{-3}s$, $T = 2.10^{-1}s$, $\tau_p = 10^{-1}s$ and $\sigma = 10^{1}m/s^{3/2}$. The dashed lines represent the analytical solutions.

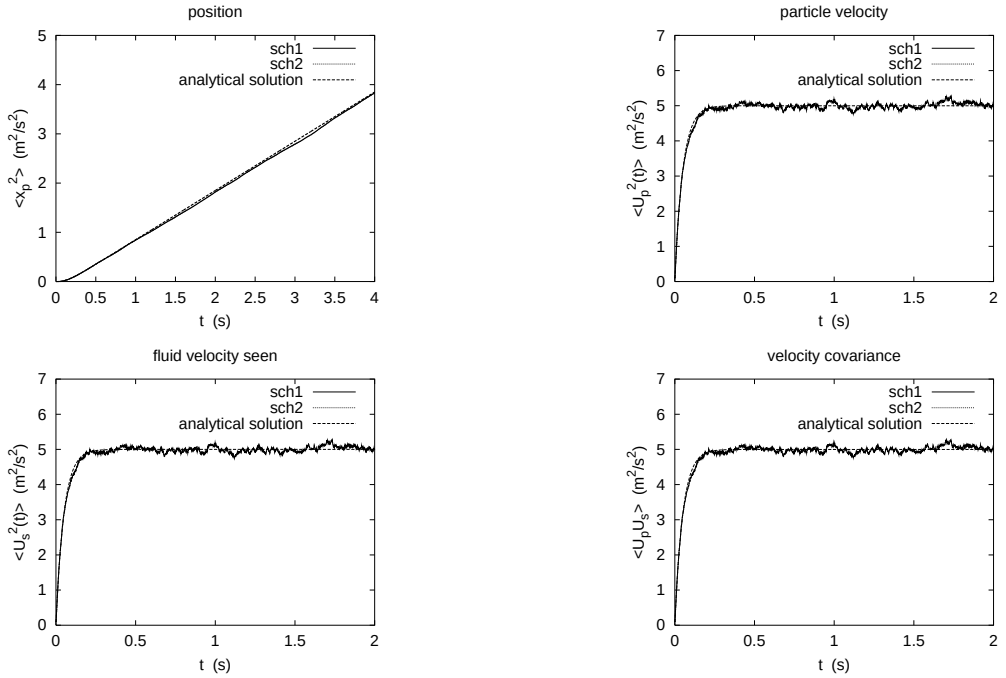

Figure 2: Numerical simulation with $N = 6000$ for system (40). Limit case (i): $\tau_p \ll \Delta t \ll T$ with $\Delta t = 10^{-3}s$, $T = 10^{-1}s$, $\tau_p = 10^{-5}s$ and $\sigma = 10^{1}m/s^{3/2}$. The dashed lines represent the analytical solutions.

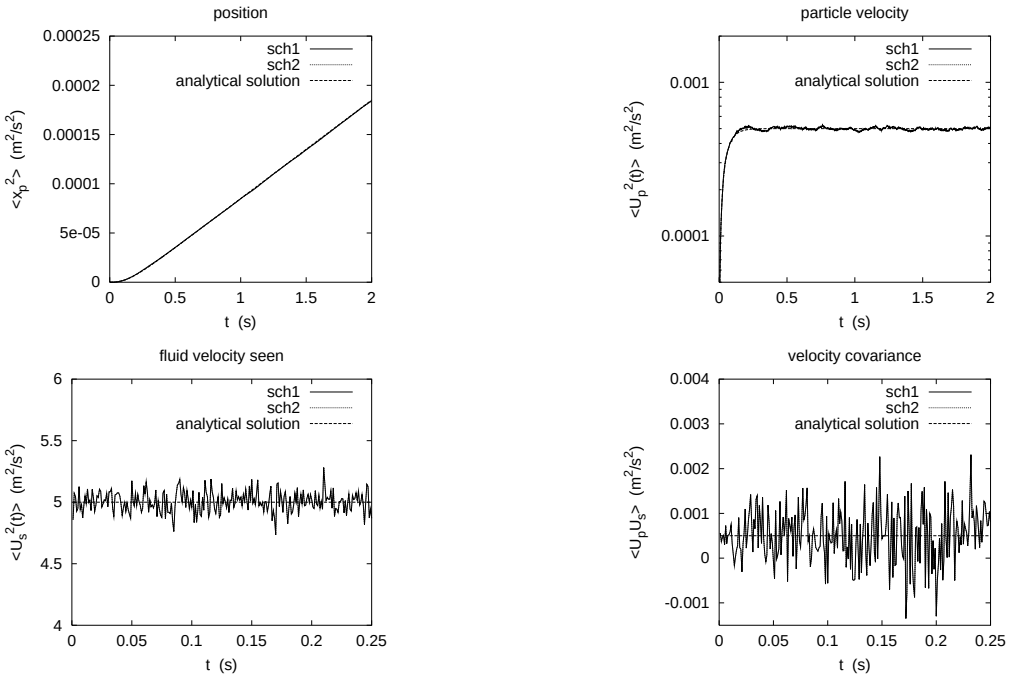

Figure 3: Numerical simulation with $N = 6000$ for system (40). Limit case (ii): $T \ll \Delta t \ll \tau_p$ with $\Delta t = 10^{-3}s$, $T = 10^{-5}s$, $\tau_p = 10^{-1}s$ and $\sigma = 10^3 m/s^{3/2}$. The dashed lines represent the analytical solutions.

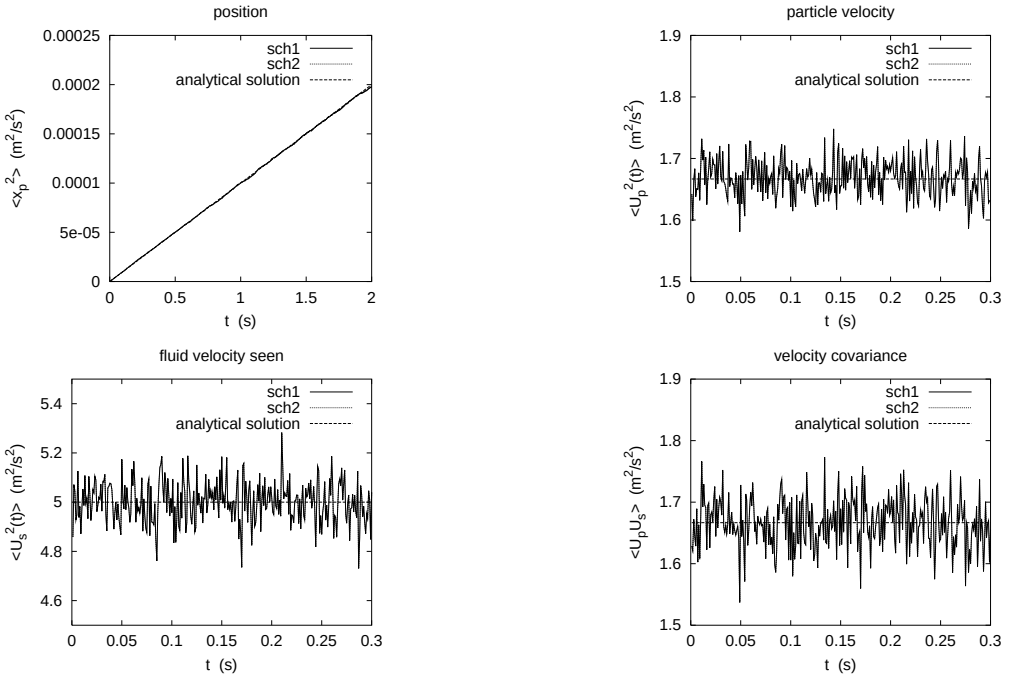

Figure 4: Numerical simulation with $N = 6000$ for system (40). Limit case (iii): $T, \tau_p \ll \Delta t$ with $\Delta t = 10^{-3}s$, $T = 10^{-5}s$, $\tau_p = 2.10^{-5}s$ and $\sigma = 10^3 m/s^{3/2}$. The dashed lines represent the analytical solutions.

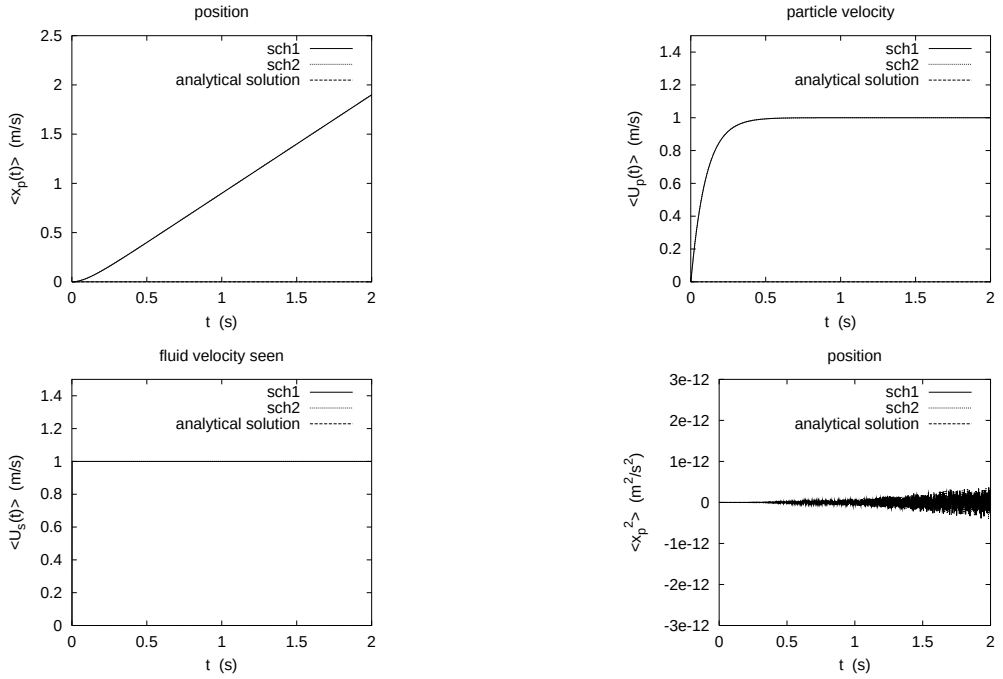

Figure 5: Numerical simulation with $N = 6000$ for system (40). Limit case (iv): $T \to 0$ with $\Delta t = 10^{-3}s$, $T = 10^{-15}s$, $\tau_p = 10^{-1}s$ and $\sigma = 10^{1}m/s^{3/2}$. The dashed lines represent the analytical solutions.

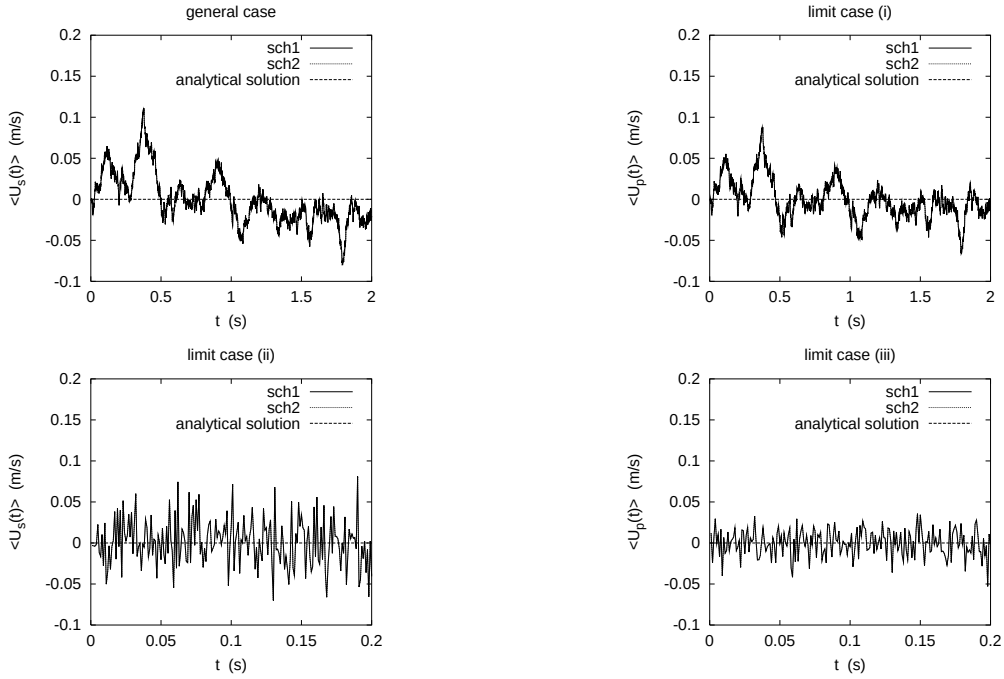

Figure 6: Numerical simulation with $N = 6000$ for system (40). Behavior of the first order moments in different cases. The dashed lines represent the analytical solutions.

Figure 7: Study of the statistical error for system (40) in the general case: $\Delta t = 10^{-3}s$, $T = 2.10^{-1}s$, $\tau_p = 10^{-1}s$ and $\sigma = 10^1 m/s^{3/2}$. Convergence curves of $\mathcal{V}_N(Z_T)$ and $\mathcal{V}_N(Z_T^2)$ with $Z_T = x_p(T)$ as a function of the number of simulations M for $N = 15000$ trajectories.

Figure 8: Study of the statistical error for system (40) in the general case: $\Delta t = 10^{-3}s$, $T = 2.10^{-1}s$, $\tau_p = 10^{-1}s$ and $\sigma = 10^1 m/s^{3/2}$. Independence of the numerical results to the time step Δt for $N = 15000$ et $M = 200$ and $Z_T = x_p(t)$.

Figure 9: Study of the discretisation error in the general case. The coefficients of system (43) are given by: $\alpha_0 = 0.5$, $a = 200.0$, $b = 0.25$, $\sigma_0 = 50.0$, and $p = -1.2$. For sch1: $N = 3.10^4$, $M = 100$ and $T = 2.4\,s$. For sch2: $N = 9.10^5$, $M = 200$ and $T = 3.2\,s$.

Figure 10: Study of the discretisation error in the general case. The coefficients of system (43) are given by: $\alpha_0 = 0.5$, $a = 200.0$, $b = 250.0$, $\sigma_0 = 50.0$, et $p = -1.2$. For sch1: $N = 3.10^4$, $M = 100$ and $T = 2.4\,s$. For sch2: $N = 9.10^5$, $M = 200$ and $T = 3.2\,s$.

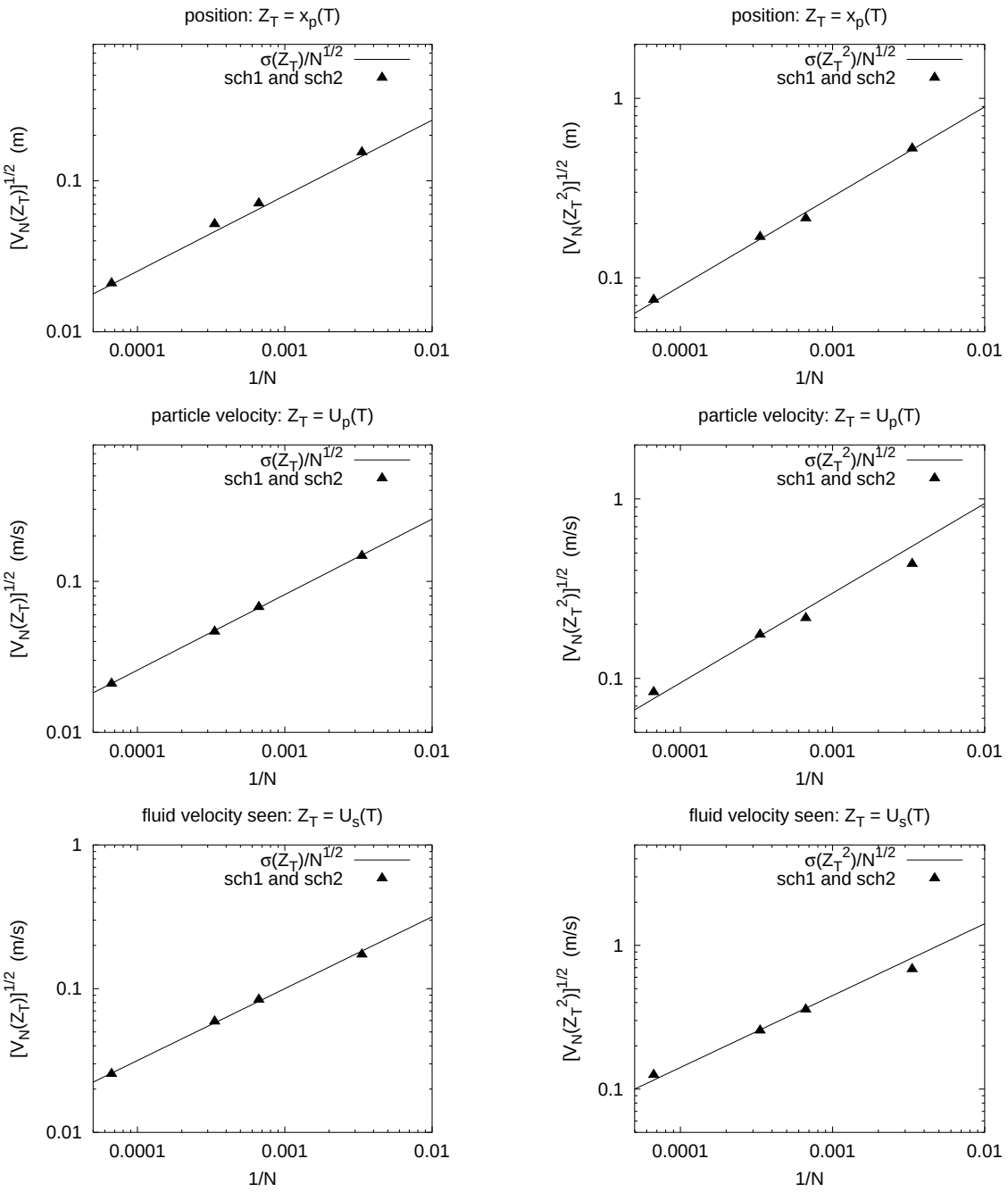

Figure 11: Study of the statistical error for system (40) in the general case: $\Delta t = 10^{-3}s$, $T = 2.10^{-1}s$, $\tau_p = 10^{-1}s$ and $\sigma = 10^{1}m/s^{3/2}$. Convergence curves for $\sqrt{\mathcal{V}_N(Z_T)}$ and $\sqrt{\mathcal{V}_N(Z_T^2)}$ as a function of the number of trajectories N.

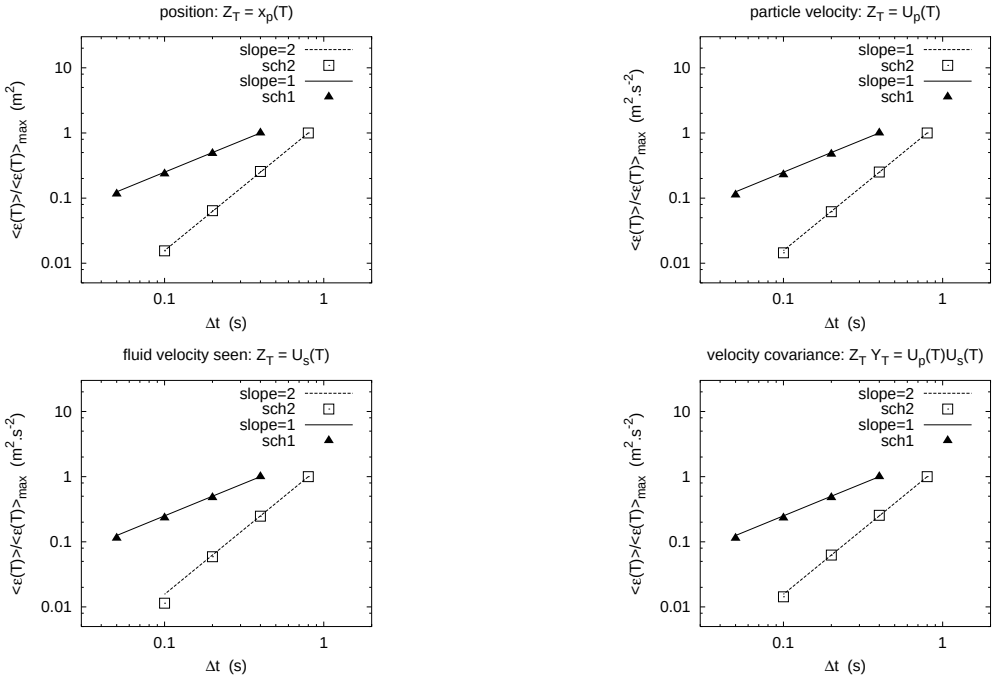

Figure 12: Study of the discretisation error in the general case. The coefficients of system (43) are given by: $\alpha_0 = 0.5$, $a = 0.1$, $b = 0.25$, $\sigma_0 = 0.5$, and $p = -1.2$. For sch1: $N = 3.10^4$, $M = 100$ and $T = 2.4\,s$. For sch2: $N = 9.10^5$, $M = 200$ and $T = 3.2\,s$.

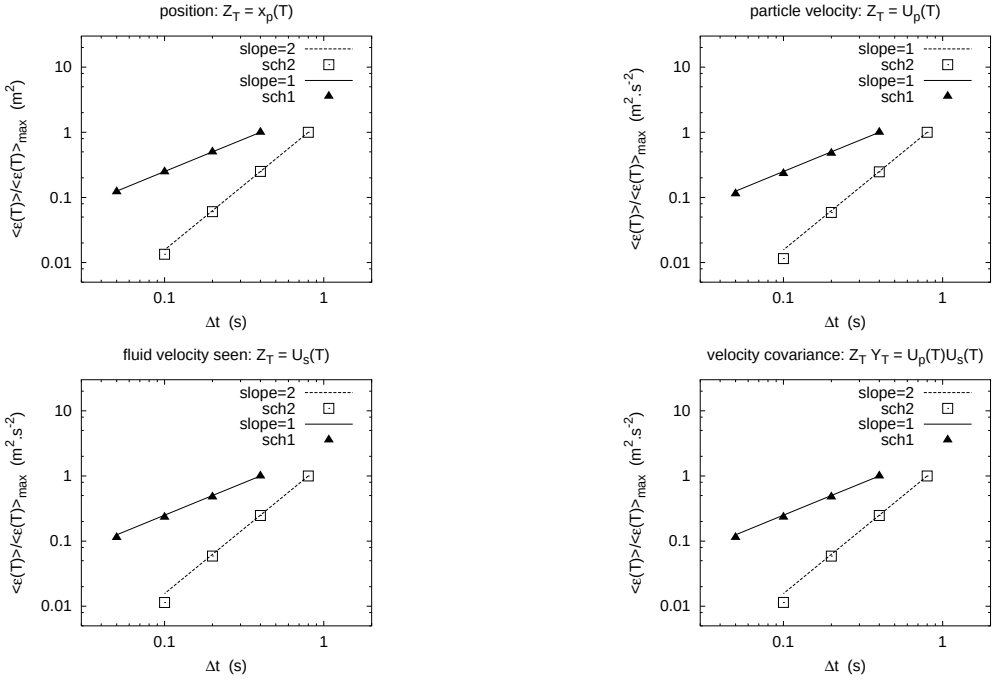

Figure 13: Study of the discretisation error in the general case. The coefficients of system (43) are given by: $\alpha_0 = 0.5$, $a = 0.1$, $b = 250$, $\sigma_0 = 0.5$, and $p = -1.2$. For sch1: $N = 3.10^4$, $M = 100$ and $T = 2.4\,s$. For sch2: $N = 9.10^5$, $M = 200$ and $T = 3.2\,s$.

Table 1: Analytical solutions to system (3) for time-independent coefficients.

$$x_{p,i}(t) = x_{p,i}(t_0) + U_{p,i}(t_0)\tau_p[1-\exp(-\Delta t/\tau_p)] + U_{s,i}(t_0)\,\theta_i\{T_i[1-\exp(-\Delta t/T_i)] + \tau_p[\exp(-\Delta t/\tau_p)-1]\}$$
$$+ [C_i(\mathrm{x}_p)T_i]\{\Delta t - \tau_p[1-\exp(-\Delta t/\tau_p)] - \theta_i(T_i[1-\exp(-\Delta t/T_i)] + \tau_p[\exp(-\Delta t/\tau_p)-1]\} + \mathcal{A}_i(\mathrm{x}_p)\tau_p\{\Delta t - \tau_p[1-\exp(-\Delta t/\tau_p)]\} + \Omega_i(t), \tag{B.2}$$

$$U_{p,i}(t) = U_{p,i}(t_0)\exp(-\Delta t/\tau_p) + U_{s,i}(t_0)\,\theta_i[\exp(-\Delta t/T_i) - \exp(-\Delta t/\tau_p)]$$
$$+ [C_i(\mathrm{x}_p)T_i]\{[1-\exp(-\Delta t/\tau_p)] - \theta_i[\exp(-\Delta t/T_i) - \exp(-\Delta t/\tau_p)]\} + \mathcal{A}_i\tau_p[1-\exp(-\Delta t/\tau_p)] + \Gamma_i(t), \tag{B.3}$$

$$U_{s,i}(t) = U_{s,i}(t_0)\exp(-\Delta t/T_i) + C_i(\mathrm{x}_p)T_i[1-\exp(-\Delta t/T_i)] + \gamma_i(t), \tag{B.4}$$

with $\quad \theta_i = \dfrac{T_i}{T_i - \tau_p} \quad$ and $\quad \Delta t = t - t_0.$

The stochastic integrals $\gamma_i(t)$, $\Gamma_i(t)$, $\Omega_i(t)$ are given by:

$$\gamma_i(t) = \sum_j \sigma_{ij}(\mathrm{x}_p)\exp(-t/T_i)\int_{t_0}^{t}\exp(s/T_i)\,dW_j(s), \tag{B.5}$$

$$\Gamma_i(t) = \frac{1}{\tau_p}\exp(-t/\tau_p)\int_{t_0}^{t}\exp(s/\tau_p)\,\gamma_i(s)\,ds, \tag{B.6}$$

$$\Omega_i(t) = \int_{t_0}^{t}\Gamma_i(s)\,ds. \tag{B.7}$$

By resorting to stochastic integration by parts, $\gamma_i(t)$, $\Gamma_i(t)$, $\Omega_i(t)$ can be written:

$$\gamma_i(t) = \sum_j \sigma_{ij}(\mathrm{x}_p)\,\exp(-t/T_i)\int_{t_0}^{t}\exp(s/T_i)\,dW_j(s), \tag{B.8}$$

$$\Gamma_i(t) = \theta_i\sum_j \sigma_{ij}(\mathrm{x}_p)\left[\exp(-t/T_i)\int_{t_0}^{t}\exp(s/T_i)\,dW_j(s) - \exp(-t/\tau_p)\int_{t_0}^{t}\exp(s/\tau_p)\,dW_j(s)\right], \tag{B.9}$$

$$\Omega_i(t) = \theta_i\sum_j \sigma_{ij}(\mathrm{x}_p)\left\{(T_i-\tau_p)\int_{t_0}^{t}dW_j(s) - \left[T_i\exp(-t/T_i)\int_{t_0}^{t}\exp(s/T_i)\,dW_j(s) - \tau_p\exp(-t/\tau_p)\int_{t_0}^{t}\exp(s/\tau_p)\,dW_j(s)\right]\right\}. \tag{B.10}$$

Table 2: Derivation of the covariance matrix for constant coefficients.

$$\langle \gamma_i^2(t) \rangle = \breve{\sigma}_i^2 \, \frac{T_i}{2} \left[1 - \exp(-2\Delta t/T_i) \right] \quad \text{where} \quad \breve{\sigma}_i^2 = \sum_j \sigma_{ij}^2 \tag{B.11}$$

$$\langle \Gamma_i^2(t) \rangle = \breve{\sigma}_i^2 \, \theta_i^2 \left\{ \frac{T_i}{2} [1 - \exp(-2\Delta t/T_i)] - \frac{2\tau_p T_i}{T_i + \tau_p} [1 - \exp(-\Delta t/T_i) \exp(-\Delta t/\tau_p)] + \frac{\tau_p}{2} [1 - \exp(-2\Delta t/\tau_p)] \right\} \tag{B.12}$$

$$\begin{aligned} \frac{1}{\breve{\sigma}_i^2 \, \theta_i^2} \langle \Omega_i^2(t) \rangle = {} & (T_i - \tau_p)^2 \Delta t + \frac{T_i^3}{2} [1 - \exp(-2\Delta t/T_i)] + \frac{\tau_p^3}{2} [1 - \exp(-2\Delta t/\tau_p)] - 2T_i^2 (T_i - \tau_p) [1 - \exp(-\Delta t/T_i)] \\ & + 2\tau_p^2 (T_i - \tau_p) [1 - \exp(-\Delta t/\tau_p)] - 2 \frac{T_i^2 \tau_p^2}{T_i + \tau_p} [1 - \exp(-\Delta t/T_i) \exp(-\Delta t/\tau_p)] \end{aligned} \tag{B.13}$$

$$\langle \gamma_i(t) \, \Gamma_i(t) \rangle = \breve{\sigma}_i^2 \, \theta_i \, T_i \left\{ \frac{1}{2} [1 - \exp(-2\Delta t/T_i)] - \frac{\tau_p}{T_i + \tau_p} [1 - \exp(-\Delta t/T_i) \exp(-\Delta t/\tau_p)] \right\} \tag{B.14}$$

$$\langle \gamma_i(t) \, \Omega_i(t) \rangle = \breve{\sigma}_i^2 \, \theta_i \, T_i \left\{ (T_i - \tau_p) [1 - \exp(-\Delta t/T_i)] - \frac{T_i}{2} [1 - \exp(-2\Delta t/T_i)] + \frac{\tau_p^2}{T_i + \tau_p} [1 - \exp(-\Delta t/T_i) \exp(-\Delta t/\tau_p)] \right\} \tag{B.15}$$

$$\begin{aligned} \frac{1}{\breve{\sigma}_i^2 \, \theta_i^2} \langle \Gamma_i(t) \, \Omega_i(t) \rangle = {} & (T_i - \tau_p) \{ T_i [1 - \exp(-\Delta t/T_i)] - \tau_p [1 - \exp(-\Delta t/\tau_p)] \} - \frac{T_i^2}{2} [1 - \exp(-2\Delta t/T_i)] - \frac{\tau_p^2}{2} [1 - \exp(-2\Delta t/\tau_p)] \\ & + T_i \tau_p \left[1 - \exp(-\Delta t/T_i) \exp(-\Delta t/\tau_p) \right] \end{aligned} \tag{B.16}$$

Table 3: Weak first order scheme (Euler scheme): sch1

Numerical integration of the system :

$$x_{p,i}^{n+1} = x_{p,i}^n + A\,U_{p,i}^n + B\,U_{s,i}^n + C\,[T_i^n C_i^n] + \mathcal{A}_i^n \tau_p^n\,(\Delta t - A) + \Omega_i^n,$$
$$U_{s,i}^{n+1} = U_{s,i}^n\,\exp(-\Delta t/T_i^n) + [T_i^n C_i^n][1 - \exp(-\Delta t/T_i^n)] + \gamma_i^n,$$
$$U_{p,i}^{n+1} = U_{p,i}^n\,\exp(-\Delta t/\tau_p^n) + D\,U_{s,i}^n + [T_i^n C_i^n](E - D) + \mathcal{A}_i \tau_p^n E + \Gamma_i^n.$$

The coefficients A, B, C, D and E are given by :

$$A = \tau_p^n\,[1 - \exp(-\Delta t/\tau_p^n)],$$
$$B = \theta_i^n\,[T_i^n(1 - \exp(-\Delta t/T_i^n) - A] \quad \text{with} \quad \theta_i^n = T_i^n/(T_i^n - \tau_p^n),$$
$$C = \Delta t - A - B,$$
$$D = \theta_i^n[\exp(-\Delta t/T_i^n) - \exp(-\Delta t/\tau_p^n)],$$
$$E = 1 - \exp(-\Delta t/\tau_p^n).$$

The stochastic integrals γ_i^n, Ω_i^n, Γ_i^n are simulated by :

$$\gamma_i^n = P_{11}\,\mathcal{G}_{1,i},$$
$$\Omega_i^n = P_{21}\,\mathcal{G}_{1,i} + P_{22}\,\mathcal{G}_{2,i}$$
$$\Gamma_i^n = P_{31}\,\mathcal{G}_{1,i} + P_{32}\,\mathcal{G}_{2,i} + P_{33}\,\mathcal{G}_{3,i},$$

where $\mathcal{G}_{1,i}$, $\mathcal{G}_{2,i}$, $\mathcal{G}_{3,i}$ are independent $\mathcal{N}(0,1)$ random variables.

The coefficients P_{11}, P_{21}, P_{22}, P_{31}, P_{32}, P_{33} are defined as :

$$P_{11} = \sqrt{\langle(\gamma_i^n)^2\rangle},$$
$$P_{21} = \frac{\langle\Omega_i^n\gamma_i^n\rangle}{\sqrt{\langle(\gamma_i^n)^2\rangle}}, \quad P_{22} = \sqrt{\langle(\Omega_i^n)^2\rangle - \frac{\langle\Omega_i^n\gamma_i^n\rangle^2}{\langle(\gamma_i^n)^2\rangle}},$$
$$P_{31} = \frac{\langle\Gamma_i^n\gamma_i^n\rangle}{\sqrt{\langle(\gamma_i^n)^2\rangle}}, \quad P_{32} = \frac{1}{P_{22}}(\langle\Omega_i^n\Gamma_i^n\rangle - P_{21}P_{31}), \quad P_{33} = \sqrt{\langle(\Gamma_i^n)^2\rangle - P_{31}^2 - P_{32}^2}).$$

Table 4: Weak second order scheme: sch2c

Prediction step:

apply the Euler scheme Sch1, see Table 3.

Correction step:

$$U_{p,i}^{n+1} = \frac{1}{2}\,U_{p,i}^{n}\,\exp(-\Delta t/\tau_p^n) + \frac{1}{2}\,U_{p,i}^{n}\,\exp(-\Delta t/\tilde{\tau}_p^{n+1}) + \frac{1}{2}\,U_{s,i}^{n} C_c(\tau_p^n,\,T_i^n) + \frac{1}{2}\,U_{s,i}^{n} C_c(\tilde{\tau}_p^{n+1},\,\tilde{T}_i^{\,n+1})$$
$$+ A_c(\tau_p^n,\,T_i^n)\,[T_i^n C_i^n] + B_c(\tilde{\tau}_p^{n+1},\,\tilde{T}_i^{n+1})\,[\tilde{T}_i^{n+1} C_i^{n+1}] + A(\Delta t,\tau_p^n)[\tau_p^n\,\mathcal{A}_i^n] + B(\Delta t,\tilde{\tau}_p^{\,n+1})[\tilde{\tau}_p^{\,n+1}\,\mathcal{A}_i^{n+1}] + \tilde{\Gamma}_i^{n+1},$$
$$U_{s,i}^{n+1} = \frac{1}{2}\,U_{s,i}^{n}\,\exp(-\Delta t/T_i^n) + \frac{1}{2}\,U_{s,i}^{n}\,\exp(-\Delta t/\tilde{T}_i^{n+1}) + A(\Delta t,\,T_i^n)\,[T_i^n C_i^n] + B(\Delta t,\,\tilde{T}_i^{n+1})\,[\tilde{T}_i^{n+1} C_i^{n+1}] + \tilde{\gamma}_i^{n+1}.$$

The coefficients $A,\ B,\ A_c,\ B_c$ et C_c are defined as : $\quad A(\Delta t, X) = -\exp(-\Delta t/X) + \left[\dfrac{1-\exp(-\Delta t/X)}{\Delta t/X}\right],$

$$B(\Delta t, X) = 1 - \left[\frac{1-\exp(-\Delta t/X)}{\Delta t/X}\right], \quad A_c(X,Y) = -\exp(-\Delta t/X) + \frac{X+Y}{\Delta t}[1-\exp(-\Delta t/X)] - \left(1+\frac{Y}{\Delta t}\right) C_c(X,Y),$$
$$B_c(X,Y) = 1 - \frac{X+Y}{\Delta t}[1-\exp(-\Delta t/X)] + \frac{Y}{\Delta t}\,C_c(X,Y), \quad C_c(X,Y) = \frac{Y}{Y-X}\,[\exp(-\Delta t/Y) - \exp(-\Delta t/X)].$$

The stochastic integrals $\tilde{\gamma}_i^{n+1}$ and $\tilde{\Gamma}_i^{n+1}$ are simulated as follows : $\tilde{\gamma}_i^{n+1} = \sqrt{\dfrac{[\sigma_i^*]^2\tilde{T}_i^{n+1}}{2}[1-\exp(-2\Delta t/\tilde{T}_i^{n+1})]}\;\mathcal{G}_{1,i},$

with $\quad \sigma_i^* = \left[A(2\,\Delta t,\,\tilde{T}_i^{n+1})\sqrt{\sum_j (\sigma_{ij}^n)^2} + B(2\,\Delta t,\,\tilde{T}_i^{n+1})\sqrt{\sum_j (\tilde{\sigma}_i^{n+1})^2}\right]\;\left[1-\exp(-2\,\Delta t/\tilde{T}_i^{n+1})\right]^{-1}.$

$$\tilde{\Gamma}_i^{n+1} = \frac{\langle\tilde{\Gamma}_i^{n+1}\tilde{\gamma}_i^{n+1}\rangle}{\langle(\tilde{\gamma}_i^{n+1})^2\rangle}\,\tilde{\gamma}_i^{n+1} + \sqrt{\langle(\tilde{\Gamma}_i^{n+1})^2\rangle - \frac{\langle\tilde{\Gamma}_i^{n+1}\tilde{\gamma}_i^{n+1}\rangle^2}{\langle(\tilde{\gamma}_i^{n+1})^2\rangle}}\;\mathcal{G}_{2,i}$$

with $\quad \langle\tilde{\Gamma}_i^{n+1}\tilde{\gamma}_i^{n+1}\rangle = \langle\Gamma_i\gamma_i\rangle(\tau_p^n,\,\tilde{T}_i^{n+1},\,\sigma_i^*) \qquad$ and $\quad \langle(\tilde{\Gamma}_i^{n+1})^2\rangle = \langle\Gamma_i^2\rangle(\tau_p^n,\,\tilde{T}_i^{n+1},\,\sigma_i^*).$

Table 5: Analytical somutions to system (40) and analytical expressions for the second order moments of $U_s(t)$ and $U_p(t)$.

By stochastic integration by parts, one has for $U_s(t)$, $U_p(t)$, $x_p(t)$:

$$U_s(t) = \frac{\sigma_0}{(\alpha_0 t+1)^k}\int_{t_0}^{t}(\alpha_0 t+1)^{k+p}\,dW(s), \tag{B.17}$$

$$U_p(t) = \frac{\sigma_0 b}{\alpha_0(n-k)}\left[\frac{1}{(\alpha_0 t+1)^k}\int_{t_0}^{t}(\alpha_0 t+1)^{k+p}\,dW(s) - \frac{1}{(\alpha_0 t+1)^n}\int_{t_0}^{t}(\alpha_0 t+1)^{n+p}\,dW(s)\right], \tag{B.18}$$

$$\begin{aligned} x_p(t) = \frac{\sigma_0 b}{\alpha_0^2(n-k)}\Bigg[&\left(\frac{1}{k-1}-\frac{1}{n-1}\right)\int_{t_0}^{t}(\alpha_0 t+1)^{p+1}\,dW(s) \\ &- \frac{(\alpha_0 t+1)^{1-k}}{k-1}\int_{t_0}^{t}(\alpha_0 t+1)^{k+p}\,dW(s) + \frac{\alpha_0 t+1)^{1-n}}{n-1}\int_{t_0}^{t}(\alpha_0 t+1)^{n+p}\,dW(s)\Bigg]. \end{aligned} \tag{B.19}$$

By resorting to Itô's calculus, $\langle U_s^2(t)\rangle$, $\langle U_p^2(t)\rangle$, $\langle U_s(t)\,U_p(t)\rangle$ can be written:

$$\langle U_s^2(t)\rangle = \frac{\sigma_0^2}{\alpha_0[2(k+p)+1]}\left[(\alpha_0 t+1)^{2p+1} - \frac{1}{(\alpha_0 t+1)^{2k}}\right], \tag{B.20}$$

$$\begin{aligned} \langle U_p^2(t)\rangle = \frac{1}{\alpha_0}\left[\frac{\sigma_0^2}{\alpha_0[2(k+p)+1]}\right]^2 \times \Bigg\{ &\frac{1}{2(k+p)+1}\times \\ \left[(\alpha_0 t+1)^{2p+1} - \frac{1}{(\alpha_0 t+1)^{2k}}\right] &- \frac{2}{k+2p+n+1}\left[(\alpha_0 t+1)^{2p+1} - \frac{1}{(\alpha_0 t+1)^{n+k}}\right] \\ &+ \frac{1}{2(n+p)+1}\left[(\alpha_0 t+1)^{2p+1} - \frac{1}{(\alpha_0 t+1)^{2n}}\right]\Bigg\}, \end{aligned} \tag{B.21}$$

$$\langle U_s(t)U_p(t)\rangle = \frac{\sigma_0^2 b}{\alpha_0^2(n-k)}\left\{\frac{1}{2(k+p)+1}\left[(\alpha_0 t+1)^{2p+1} - \frac{1}{(\alpha_0 t+1)^{2k}}\right] - \frac{1}{k+2p+n+1}\left[(\alpha_0 t+1)^{2p+1} - \frac{1}{(\alpha_0 t+1)^{n+k}}\right]\right\}.$$

Eqs. (B.18) to (B.22) are valid provided that: $n \neq k$, $k \neq 1$, $n \neq 1$, $2(k+p)+1 \neq 0$, $2(n+p)+1 \neq 0$, $n+2p+k+1 \neq 0$.

Table 6: Analytical expressions for the second order moment of $x_p(t)$.

Eq. (B.19) is rewritten as $x_p(t) = \left[\frac{\sigma_0 b}{\alpha_0^2(n-k)}\right][I_1 + I_2 + I_3]$ and the second order moment becomes: (B.22)

$$\langle x_p^2(t)\rangle = \left[\frac{\sigma_0 b}{\alpha_0^2(n-k)}\right]^2 \left[\sum_{i=1} 3\langle I_i^2\rangle + 2\sum_{i,j=1} 3\langle I_i\, I_j\rangle\right]. \tag{B.23}$$

The expected values $\langle I_i^2\rangle$ and $\langle I_i\, I_j\rangle$ are defined as:

$$\langle I_1^2\rangle = \frac{1}{\alpha_0(2p+3)}\left[\frac{1}{k-1} - \frac{1}{n-1}\right]^2 \left[(\alpha_0 t+1)^{2p+3} - 1\right], \tag{B.24}$$

$$\langle I_2^2\rangle = \frac{1}{\alpha_0[2(k+p)+1]}\left[\frac{1}{k-1}\right]^2 \left[(\alpha_0 t+1)^{2p+3} - (\alpha_0 t+1)^{2(1-k)}\right], \tag{B.25}$$

$$\langle I_3^2\rangle = \frac{1}{\alpha_0[2(n+p)+1]}\left[\frac{1}{n-1}\right]^2 \left[(\alpha_0 t+1)^{2p+3} - (\alpha_0 t+1)^{2(1-n)}\right], \tag{B.26}$$

$$2\langle I_1 I_2\rangle = -\frac{2}{k-1}\left[\frac{1}{k-1} - \frac{1}{n-1}\right]\frac{1}{\alpha_0(k+2p+2)}\left[(\alpha_0 t+1)^{2p+3} - (\alpha_0 t+1)^{1-k}\right], \tag{B.27}$$

$$2\langle I_1 I_3\rangle = \frac{2}{n-1}\left[\frac{1}{k-1} - \frac{1}{n-1}\right]\frac{1}{\alpha_0(n+2p+2)}\left[(\alpha_0 t+1)^{2p+3} - (\alpha_0 t+1)^{1-n}\right], \tag{B.28}$$

$$2\langle I_2 I_3\rangle = -2\frac{1}{n-1}\,\frac{1}{k-1}\,\frac{1}{\alpha_0(n+2p+k+1)}\left[(\alpha_0 t+1)^{2p+3} - (\alpha_0 t+1)^{2-n-k}\right]. \tag{B.29}$$

Eqs. (B.23) to (B.29) are valid if n, k, p fulfill the conditions given in Table 5 and if one has $k+2p+2 \neq 0$ and $n+2p+2 \neq 0$.

Table 7: Numerical simulation for system (40) in the general and limit cases. General case: $\Delta t \ll T, \tau_p$. Limit case (i): $\tau_p \ll \Delta t \ll T$. Limit case (ii): $T \ll \Delta t \ll \tau_p$. Limit case (iii): $T, \tau_p \ll \Delta t$. Limit case (iv): $T \to 0$.

case	$\tau_p\ (s)$	$T\ (s)$	$\sigma\ (m/s^{3/2})$	$\Delta t\ (s)$
general case	10^{-1}	2.10^{-1}	10^{1}	10^{-3}
limit case (i)	10^{-5}	10^{-1}	10^{1}	10^{-3}
limit case (ii)	10^{-1}	10^{-5}	10^{3}	10^{-3}
limit case (iii)	2.10^{-5}	10^{-5}	10^{3}	10^{-3}
limit case (iv)	10^{-1}	10^{-15}	10^{1}	10^{-3}

Table 8: Numerical values for the parameters of system (43), (α_0, a, b, σ_0 and p), in the simulations of the general case and the different limit cases.

	α_0	a	b	σ_0	p
general case	0.5	0.1	0.25	0.5	-1.2
limit case (i)	0.5	0.1	250.	0.5	-1.2
limit case (ii)	0.5	200.	250.	50.	-1.2
limit case (iii)	0.5	200.	250.	50.	-1.2

Table 9: Numerical values for the number of trajectories N, the number of simulations M, the final time T and the time step interval $[\Delta t_{min}, \Delta t_{max}]$ in the simulations.

	N	M	$T\ (s)$	$\Delta t_{max}\ (s)$	$\Delta t_{min}\ (s)$
sch1	3.10^4	10^2	2.4	5.10^{-2}	4.10^{-1}
sch2	9.10^5	2.10^2	3.2	10^{-1}	8.10^{-1}